

Complete $\mathcal{O}(\alpha)$ QED corrections to polarized Compton scattering

A. DENNER

Paul Scherrer Institut

CH-5232 Villigen PSI, Switzerland

S. DITTMAYER

Theory Division, CERN

CH-1211 Geneva 23, Switzerland

Abstract:

The complete QED corrections of $\mathcal{O}(\alpha)$ to polarized Compton scattering are calculated for finite electron mass and including the real corrections induced by the processes $e^- \gamma \rightarrow e^- \gamma \gamma$ and $e^- \gamma \rightarrow e^- e^- e^+$. All relevant formulas are listed in a form that is well suited for a direct implementation in computer codes. We present a detailed numerical discussion of the $\mathcal{O}(\alpha)$ -corrected cross section and the left-right asymmetry in the energy range of present and future Compton polarimeters, which are used to determine the beam polarization of high-energetic e^\pm beams. For photons with energies of a few eV and electrons with SLC energies or smaller, the corrections are of the order of a few per mille. In the energy range of future e^+e^- colliders, however, they reach 1–2% and cannot be neglected in a precision polarization measurement.

1 Introduction

The sensitivity of Compton scattering, $e^\pm\gamma \rightarrow e^\pm\gamma$, to the polarization of both the electron and the photon in the initial state renders this process well suited for the determination of the polarization of electron (or positron) beams in high-energy collider experiments. Usually, in a Compton polarimeter, circularly polarized laser light is brought to collision with the high-energetic e^\pm beam, and the degree of beam polarization is deduced from the left–right asymmetry with respect to the polarization of the laser photons. The high precision of such polarization measurements, which is typically of the order of 1% [1–4], sets the necessary level of accuracy in theoretical predictions to a few per mille. Therefore, it is indispensable to control radiative corrections.

In the low-energy limit, the QED corrections to the Compton scattering cross section are known to vanish to all orders of perturbation theory [5, 6], i.e. the relative corrections are suppressed by a factor of the electron velocity β for small β . This fact, which is known as Thirring’s theorem, is due to the definition of the electromagnetic charge in the Thomson limit and electromagnetic gauge invariance. On the other hand, the relative corrections to the polarization asymmetry are not suppressed with β , since the asymmetry itself vanishes for $\beta \rightarrow 0$. Therefore, the QED corrections to the asymmetry are expected to be of the order of α/π times some numerical factor, i.e. of 0.1–1%, even for small scattering energies.

The first calculation of the virtual and real soft-photonic QED corrections in $\mathcal{O}(\alpha)$ was performed by Brown and Feynman [7] for the unpolarized cross section in 1952. In the same year, the amplitudes for the corresponding hard-photonic bremsstrahlung, so-called double Compton scattering, $e^- \gamma \rightarrow e^- \gamma \gamma$, were given by Mandl and Skyrme [8]. The investigation of radiative corrections to polarized particles started much later: in 1972 the one-loop and real soft-photonic corrections were presented by Milton, Tsai, and De Raad [9]. The helicity amplitudes for hard-photon radiation were given by G3ngora-T. and Stuart [10] in 1989. In the same year the first numerical evaluation of polarized Compton scattering was published by H. Veltman [11], who, in particular, studied the impact of QED corrections on the beam-polarization measurement at SLAC. A recent evaluation by Swartz [12], which is based on the (corrected) formulas of Refs. [9, 10], could not confirm Veltman’s results. Even though both authors find corrections of the order of 0.1–0.2% for the SLAC polarimeter, which is small with respect to the experimental uncertainty of about 0.7% [1], it is necessary to settle this issue. For a Next Linear Collider (NLC) with e^\pm beams of 500 GeV, Swartz finds QED corrections of 1–2%, definitely requiring their inclusion in the determination of the beam polarization.

In view of this situation, we have performed a completely independent calculation of the $\mathcal{O}(\alpha)$ QED corrections to polarized Compton scattering, the analytical and numerical results of which are presented in this paper. In order to facilitate the use of our formulas, the presentation is held at a rather detailed level. As done in Ref. [12], we also include the real corrections induced by the process $e^- \gamma \rightarrow e^- e^- e^+$, which will be relevant at beam energies of future colliders if not the photons but the electrons of the final state are detected.

Because Compton scattering is a pure QED process in lowest order, the electroweak radiative corrections can be split into a QED part and a genuinely weak part in a gauge-

invariant way, just by selecting the QED diagrams and the remaining ones at each loop level. Since Thirring's low-energy theorem is also valid in the electroweak Standard Model [6], also the weak corrections vanish in the low-energy limit. At any centre-of-mass (CM) energy E_{CM} that is far below the electroweak bosons' masses M_W , etc., the weak corrections are suppressed by factors of E_{CM}^2/M_W^2 . This feature can be observed directly by inspecting the weak one-loop corrections that were explicitly calculated in Refs. [13,14]. Owing to this suppression, the weak corrections are irrelevant for a Compton polarimeter, where $E_{\text{CM}} = \mathcal{O}(m_e)$ and thus $E_{\text{CM}}^2 \ll M_W^2$. However, for CM energies above the weak scale M_W , i.e. in the range of future $e^\pm\gamma$ colliders, these corrections become large, reaching 5–10% in the TeV range.

This article is organized as follows: in Sect. 2 we set some conventions and present the necessary formulas for the lowest-order predictions. Section 3 contains our analytical results for the virtual one-loop corrections. The correction factor for soft-photonic bremsstrahlung as well as the helicity amplitudes for $e^-\gamma \rightarrow e^-\gamma\gamma, e^-e^-e^+$ are given in Sect. 4. In Sect. 5 we discuss our numerical results, which include studies for Compton polarimeters for e^\pm -beam energies of 4–8 GeV (CEBAF), 50 GeV (SLAC), and 500 GeV (NLC).

2 Conventions and lowest-order cross-sections

The momenta and polarizations for the Compton process are assigned as follows:

$$e^-(p, \sigma) + \gamma(k, \lambda) \longrightarrow e^-(p', \sigma') + \gamma(k', \lambda'), \quad (2.1)$$

where the helicities take the values $\sigma, \sigma' = \pm 1/2$ and $\lambda, \lambda' = \pm 1$. For brevity the helicities are often indicated by their sign. We have chosen incoming electrons for definiteness; the results for incoming positrons follow by charge conjugation.

We first specify the kinematics in the CM system, where all momenta are fixed by the energy of one particle and the scattering angle in the scattering plane. Denoting the photon energy by E_γ , the electron energy E_e and the electron velocity β are given by

$$E_e = \sqrt{E_\gamma^2 + m_e^2}, \quad \beta = E_\gamma/E_e. \quad (2.2)$$

Identifying the beam axes with the z direction and taking the x - z plane as scattering plane, the momenta read

$$\begin{aligned} p^\mu &= E_e(1, 0, 0, \beta), & k^\mu &= E_\gamma(1, 0, 0, -1), \\ p'^\mu &= E_e(1, \beta \sin \theta, 0, \beta \cos \theta), & k'^\mu &= E_\gamma(1, -\sin \theta, 0, -\cos \theta). \end{aligned} \quad (2.3)$$

The Mandelstam variables are defined as usual:

$$\begin{aligned} s &= (p + k)^2 = (p' + k')^2 = E_{\text{CM}}^2 = (E_e + E_\gamma)^2, \\ t &= (p - p')^2 = (k - k')^2 = -4E_\gamma^2 \sin^2(\frac{\theta}{2}), \\ u &= (p - k')^2 = (p' - k)^2 = (E_e - E_\gamma)^2 - 4E_\gamma^2 \cos^2(\frac{\theta}{2}). \end{aligned} \quad (2.4)$$

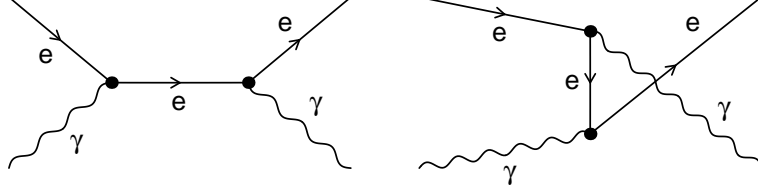


Figure 1: Tree diagrams for $e^- \gamma \rightarrow e^- \gamma$

Moreover, it is convenient to introduce the shorthands

$$\begin{aligned}
 s_m &= s - m_e^2 = 2E_\gamma \sqrt{s}, & u_m &= u - m_e^2 = -2E_\gamma \left[2E_\gamma \cos^2 \left(\frac{\theta}{2} \right) + \frac{m_e^2}{\sqrt{s}} \right], \\
 t_m &= t - 4m_e^2, & r &= \sqrt{m_e^4 - su} = s_m \cos \left(\frac{\theta}{2} \right).
 \end{aligned}
 \tag{2.5}$$

For the photon polarization vectors of helicity eigenstates we choose

$$\begin{aligned}
 \varepsilon^\mu(k, \lambda = \pm 1) &= \frac{1}{\sqrt{2}}(0, 1, \mp i, 0), \\
 \varepsilon'^{\mu}(k', \lambda' = \pm 1) &= \frac{1}{\sqrt{2}}(0, \cos \theta, \pm i, -\sin \theta).
 \end{aligned}
 \tag{2.6}$$

For the helicity eigenspinors of the electrons we refer to Ref. [15]. The discrete symmetries of QED, actually parity and the combination of charge conjugation and time reversal, reduce the number of independent helicity amplitudes for $e^- \gamma \rightarrow e^- \gamma$ to six. In lowest order these amplitudes, $\mathcal{M}_0(\sigma, \lambda, \sigma', \lambda')$, receive contributions from the two tree diagrams shown in Fig. 1 and are given by

$$\begin{aligned}
 \mathcal{M}_0(\pm\pm\pm\pm) &= 8\pi\alpha \frac{r(s_m^2 + m_e^2 t)}{s_m^2 u_m}, \\
 \mathcal{M}_0(\pm\mp\pm\mp) &= 8\pi\alpha \frac{r^3}{s_m^2 u_m}, \\
 \mathcal{M}_0(\pm\mp\mp\pm) &= \pm 8\pi\alpha \frac{m_e s t \sqrt{-t}}{s_m^2 u_m}, \\
 \mathcal{M}_0(\pm\mp\mp\mp) &= \mathcal{M}_0(\pm\pm\mp\pm) = \pm 8\pi\alpha \frac{m_e r^2 \sqrt{-t}}{s_m^2 u_m}, \\
 \mathcal{M}_0(\pm\pm\pm\mp) &= \mathcal{M}_0(\pm\mp\pm\pm) = 8\pi\alpha \frac{m_e^2 r t}{s_m^2 u_m}, \\
 \mathcal{M}_0(\pm\pm\mp\mp) &= \pm 8\pi\alpha \frac{m_e^3 t \sqrt{-t}}{s_m^2 u_m},
 \end{aligned}
 \tag{2.7}$$

where α is the fine-structure constant.

Usually, for $e^\pm \gamma$ collisions the CM system and the laboratory (LAB) frame do not coincide. Throughout this paper we assume that the CM and LAB frames are related by

a boost along the beam axes. This boost is completely fixed by specifying the energies \bar{E}_e and \bar{E}_γ of the incoming electron and photon in the LAB frame. Actually, in practice the angle between the incoming beams in the LAB system deviates from 180° by a very small angle α_c of some mrad, but the impact of this effect is negligible for present and future polarimeters. More details about the situation with non-zero α_c are given in the appendix.

In terms of LAB variables, which are marked by bars, the particle momenta read

$$\begin{aligned} p^\mu &= \bar{E}_e(1, 0, 0, \bar{\beta}), & k^\mu &= \bar{E}_\gamma(1, 0, 0, -1), \\ p'^\mu &= \bar{E}'_e(1, \bar{\beta}' \sin \bar{\theta}'_e, 0, \bar{\beta}' \cos \bar{\theta}'_e), & k'^\mu &= \bar{E}'_\gamma(1, \sin \bar{\theta}'_\gamma, 0, \cos \bar{\theta}'_\gamma), \end{aligned} \quad (2.8)$$

where

$$\bar{\beta} = \sqrt{1 - m_e^2/\bar{E}_e^2}, \quad \bar{\beta}' = \sqrt{1 - m_e^2/\bar{E}'_e^2} \quad (2.9)$$

are the velocities of the respective electrons. The relation between quantities in the different frames are most conveniently written in terms of the boost parameters

$$\beta_b = \frac{\bar{\beta}\bar{E}_e - \bar{E}_\gamma}{\bar{E}_e + \bar{E}_\gamma}, \quad \gamma_b = \frac{1}{\sqrt{1 - \beta_b^2}} = \frac{\bar{E}_e + \bar{E}_\gamma}{\sqrt{s}}, \quad (2.10)$$

where

$$s = m_e^2 + 2\bar{E}_\gamma\bar{E}_e(1 + \bar{\beta}). \quad (2.11)$$

The photon energy in the CM system is given by

$$E_\gamma = \bar{E}_\gamma\gamma_b(1 + \beta_b), \quad (2.12)$$

from which E_e and β follow through (2.2). The scattering angle θ in the CM system is related to the energy \bar{E}'_e of the outgoing electron and to the energy \bar{E}'_γ of the outgoing photon in the LAB frame by

$$\cos \theta = \frac{\bar{E}'_e - \gamma_b E_e}{E_\gamma \gamma_b \beta_b} = \frac{\gamma_b E_\gamma - \bar{E}'_\gamma}{E_\gamma \gamma_b \beta_b}. \quad (2.13)$$

The extreme values of \bar{E}'_e and \bar{E}'_γ correspond to the scattering into forward and backward directions:

$$\begin{aligned} \bar{E}'_{e,\max} &= \bar{E}_e + \bar{E}_\gamma - \bar{E}'_{\gamma,\min} = \bar{E}_e, \\ \bar{E}'_{\gamma,\max} &= \bar{E}_e + \bar{E}_\gamma - \bar{E}'_{e,\min} = \frac{E_\gamma^2}{E_\gamma}, \end{aligned} \quad (2.14)$$

provided that $\beta_b < \beta$. This condition, which is obviously fulfilled for Compton polarimeters, ensures that the scattered electron cannot be at rest in the LAB frame.

Note that the amplitudes (2.7) refer to helicity eigenstates in the CM frame, and that the property of being a helicity eigenstate is frame-dependent for massive particles. In our case, however, the incoming electron is in a state of definite helicity both in the CM and in the LAB system, because the boost that relates the two frames goes along the direction of flight for this particle. The outgoing electron is in general not in a helicity eigenstate

in the LAB frame. In practice this does not matter, as the spins of the outgoing particles are not measured.

The basic observable is the differential lowest-order cross section in the CM system,

$$\frac{d\sigma_0(P_e, P_\gamma)}{d\cos\theta} = \frac{1}{32\pi s} \sum_{\sigma, \lambda, \sigma', \lambda'} \frac{1}{4} (1 + 2\sigma P_e)(1 + \lambda P_\gamma) |\mathcal{M}_0(\sigma, \lambda, \sigma', \lambda')|^2, \quad (2.15)$$

where P_e and P_γ denote the respective degrees of beam polarization, which do not change by the boost to the LAB frame. Using (2.13) this leads us, for instance, directly to the electron-energy distribution in the LAB frame:

$$\frac{d\sigma_0(P_e, P_\gamma)}{d\bar{E}'_e} = \frac{1}{E_\gamma \gamma_b \beta_b} \frac{d\sigma_0(P_e, P_\gamma)}{d\cos\theta} \Big|_{\cos\theta = \frac{\bar{E}'_e - \gamma_b E_e}{E_\gamma \gamma_b \beta_b}}. \quad (2.16)$$

The most important quantity for a Compton polarimeter is the polarization asymmetry $A_{\text{LR}}(P_e)$ with respect to incoming laser photons of opposite polarization:

$$A_{\text{LR}}(P_e) = \frac{\Delta\sigma(P_e, -1) - \Delta\sigma(P_e, +1)}{\Delta\sigma(P_e, -1) + \Delta\sigma(P_e, +1)}, \quad (2.17)$$

where the defining cross section $\Delta\sigma(P_e, P_\gamma)$ can be the integrated cross section or any distribution measured by the detector. As long as effects of the weak interaction can be neglected (see introduction), parity is an exact symmetry, and we have $\Delta\sigma(P_e, P_\gamma) = \Delta\sigma(-P_e, -P_\gamma)$. In this case we get

$$A_{\text{LR}}(P_e) = P_e A_{\text{LR}}(+1), \quad (2.18)$$

and P_e can be determined by the measured value of $A_{\text{LR}}(P_e)$ divided by the theoretical prediction for $A_{\text{LR}} \equiv A_{\text{LR}}(+1)$.

Note that (2.15) makes use of rotational invariance with respect to the beam axes, which is also assumed in the above treatment of the kinematics. This procedure is adequate for helicity states, but should be generalized if one is interested in transverse polarizations, which are not considered in this paper. It is quite easy to deduce the amplitudes for any polarization configuration from our helicity amplitudes, both for the lowest order and for the corrections described in the next sections.

3 Virtual corrections

For the virtual corrections the kinematics is the same as in lowest order. Lowest-order amplitudes and loop amplitudes simply add up to the full amplitudes \mathcal{M} . The squared amplitudes $|\mathcal{M}|^2$ are expanded in α . In $\mathcal{O}(\alpha)$ precision this leads to $|\mathcal{M}|^2 = |\mathcal{M}_0|^2 + 2\text{Re}\{\mathcal{M}_0\mathcal{M}_1^*\} + \mathcal{O}(\alpha^2)$, where \mathcal{M}_1 is the sum of all one-loop diagrams. Therefore, in one-loop approximation the virtual correction to the differential Born cross section (2.15) in the CM system reads

$$\frac{d\sigma_V(P_e, P_\gamma)}{d\cos\theta} = \frac{1}{32\pi s} \sum_{\sigma, \lambda, \sigma', \lambda'} \frac{1}{4} (1 + 2\sigma P_e)(1 + \lambda P_\gamma) 2\text{Re}\{\mathcal{M}_0(\sigma, \lambda, \sigma', \lambda')\mathcal{M}_1^*(\sigma, \lambda, \sigma', \lambda')\}. \quad (3.1)$$

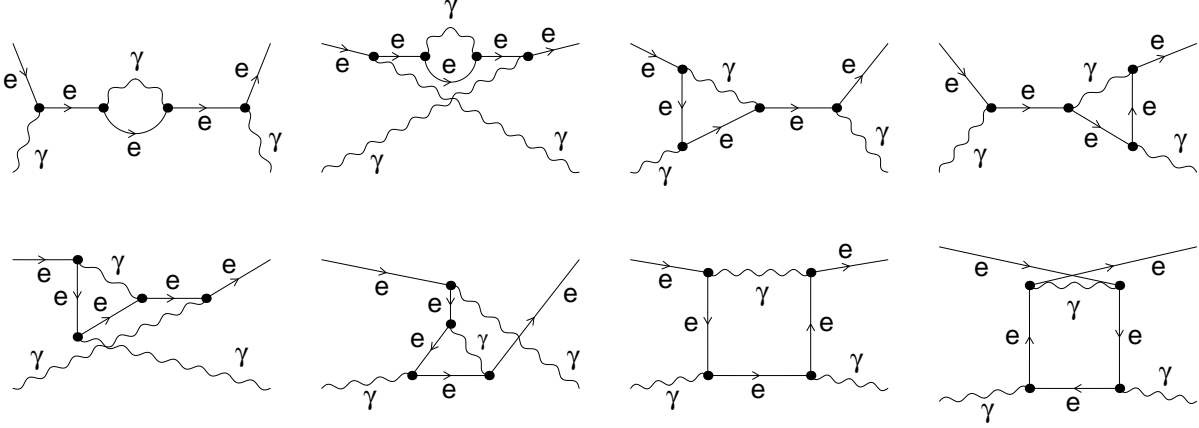


Figure 2: One-loop QED diagrams for $e^- \gamma \rightarrow e^- \gamma$

The transition to other distributions like the one of (2.16) is obtained as in lowest order.

The one-loop diagrams, which are depicted in Fig. 2, have been calculated using the standard technique described in Ref. [16]. This means that one-loop tensor integrals are algebraically reduced to scalar integrals à la Passarino and Veltman [17], and the scalar integrals are analytically integrated using the general methods described in Ref. [18]. The algebraic part of the calculation has been performed in two different ways. The first calculation is based on the computer algebra packages *FeynArts* [19] and *FeynCalc* [20]; the former generates the one-loop amplitudes, the latter performs several kinds of algebraic manipulations (contractions, application of Dirac's equation, etc.) and reduces the tensor integrals to scalar integrals. The second calculation makes direct use of the existing one-loop results for the process $\gamma\gamma \rightarrow t\bar{t}$ [21], which were derived once with and once without *FeynCalc*. The reaction $\gamma\gamma \rightarrow t\bar{t}$ is related to Compton scattering via crossing symmetry, i.e. one simply has to reverse the momenta of the anti-top quark and of one of the photons, to replace the corresponding spinor and polarization vector, and to substitute the top-quark parameters (charge, mass, colour) by the corresponding parameters of the electron. The final step of evaluating the spinor chains for definite helicity states has also been carried out in different ways.

In QED the one-loop amplitudes $\mathcal{M}_1(\sigma, \lambda, \sigma', \lambda')$ are related by the same discrete symmetries as the Born amplitudes (2.7). In terms of scalar integrals the independent \mathcal{M}_1 are given by

$$\begin{aligned}
\mathcal{M}_1(++++) = & 2\alpha^2 \frac{r}{s_m} \left\{ \frac{s_m^2 u + m_e^2 t^2 - 2m_e^4 t}{su_m u} + 4m_e^2 \frac{s_m^2 + m_e^2 t}{s_m u_m} B' + \frac{2t}{t_m} B_{mm}(t) \right. \\
& + m_e^2 \frac{5s^2 - 2m_e^2 s + m_e^4}{ss_m^2} B_{0m}(s) + \frac{r^2 u + 2tu^2 + 4m_e^2 u^2 + m_e^4 t}{uu_m^2} B_{0m}(u) \\
& + \frac{1}{r^2} \left[-t(s^2 + t^2 + m_e^2 t - 9m_e^4) C_{mmm}(t) + t_m(s_m^2 - t^2 - m_e^2 t) C_{m0m}(t) \right. \\
& \quad - 2s_m[s^2 - m_e^2(4s + u)] C_{0mm}(s) - 2u_m(t^2 + 3m_e^2 s - 7m_e^4) C_{0mm}(u) \\
& \quad \left. + [s_m^3 t - m_e^2 s_m(2s_m^2 + s_m t_m - t t_m) + 2m_e^4 t^2 - 4m_e^6 t] D_{m0mm}(t, s) \right]
\end{aligned}$$

$$\begin{aligned}
& + [t^3 u_m + m_e^2(2t^3 + s_m^2 u_m - s_m u_m^2) - 2m_e^4(s_m^2 - 3u_m^2) - 4m_e^6 t] D_{m0mm}(t, u) \Big] \Big\}, \\
\mathcal{M}_1(+--+ -) &= 2\alpha^2 \frac{r}{s_m} \left\{ -\frac{u_m}{u} + 4m_e^2 \frac{r^2}{s_m u_m} B' + 2t \frac{s_m^2 + m_e^2(3s_m - u_m)}{r^2 t_m} B_{mm}(t) \right. \\
& - (s + m_e^2) \frac{s_m^2(2s_m + 3u) + 5m_e^2 s_m u_m - 2m_e^4 t}{r^2 s_m^2} B_{0m}(s) \\
& - m_e^2 \frac{3s_m u u_m^2 - 2u_m^4 - m_e^2(4r^2 u + u_m^3)}{r^2 u u_m^2} B_{0m}(u) \\
& + \frac{1}{r^4} \left[-t[2r^2 s t_m + s^2 s_m^2 + m_e^2(s_m^3 - s s_m u_m + s_m u u_m - u u_m^2)] C_{mmm}(t) \right. \\
& + t_m[s_m^3(s_m + 2t) - m_e^2 t^2(4s_m + t) - m_e^4 t^2] C_{m0m}(t) \\
& - 2s_m[s^2 t t_m - m_e^2 s s_m(3s_m + 2t) + m_e^4 s_m u_m] C_{0mm}(s) \\
& + 2u_m[r^2 s u + m_e^2 u(s_m t + u_m^2) + m_e^4(2s_m^2 + 3st)] C_{0mm}(u) \\
& + (s + m_e^2)[s^2 t^3 + m_e^2 s_m^2(2s_m^2 + 3s_m t - 2t^2) - 5m_e^4 s_m t^2 - 2m_e^6 t^2] D_{m0mm}(t, s) \\
& + [s_m^2 t u_m^3 + m_e^2 u_m(3t^3 u + t^2 u_m^2 - 5t u_m^3 - 2u_m^4) - m_e^4 u_m^2(5t^2 + 6t u_m - 4u_m^2) \\
& \left. + 2m_e^6 t^2(t - 2u)] D_{m0mm}(t, u) \right] \Big\},
\end{aligned}$$

$$\begin{aligned}
\mathcal{M}_1(+---+) &= 4\alpha^2 \frac{m_e \sqrt{-t}}{s_m} \left\{ \frac{s_m}{u_m} + 2m_e^2 \frac{st}{s_m u_m} B' + s \frac{3s - m_e^2}{s_m^2} B_{0m}(s) \right. \\
& + \frac{3su + m_e^2 s - 2m_e^4}{u_m^2} B_{0m}(u) - 2m_e^2 C_{mmm}(t) - 2m_e^2 \frac{t}{u_m} C_{0mm}(u) \\
& \left. - m_e^2 t D_{m0mm}(t, u) + (st - 3m_e^2 s + m_e^4)[D_{m0mm}(t, s) + D_{m0mm}(t, u)] \right\},
\end{aligned}$$

$$\begin{aligned}
\mathcal{M}_1(+----) &= 2\alpha^2 \frac{m_e \sqrt{-t}}{s_m} \left\{ -\frac{r^2}{u u_m} + 4m_e^2 \frac{r^2}{s_m u_m} B' + 2 \frac{s - u}{t_m} B_{mm}(t) + 4 \frac{s^2}{s_m^2} B_{0m}(s) \right. \\
& - \frac{r^2 u_m + 2u u_m^2 - 4m_e^4 u}{u u_m^2} B_{0m}(u) \\
& + \frac{1}{r^2} \left[-t(2st + u u_m - 7m_e^2 s - m_e^4) C_{mmm}(t) + t_m(2s_m^2 - u_m^2 - m_e^2 t) C_{m0m}(t) \right. \\
& - 2s_m(r^2 - 2s^2 - 2m_e^2 s) C_{0mm}(s) + 2u_m(2s + t)(u + m_e^2) C_{0mm}(u) \\
& - (s_m^3 t - s^2 t t_m - 4m_e^2 s s_m^2 - m_e^2 s t^2) D_{m0mm}(t, s) \\
& \left. + (t^2 u^2 + 2t_m u_m^3 + 4m_e^2 u u_m^2 + m_e^4 t t_m) D_{m0mm}(t, u) \right] \Big\},
\end{aligned}$$

$$\mathcal{M}_1(+++-) = 2\alpha^2 \frac{m_e^2 r}{s_m u_m} \left\{ \frac{s - u}{m_e^2} + 4m_e^2 \frac{t}{s_m} B' + 4 \frac{s u_m}{s_m^2} B_{0m}(s) + 2 \frac{(2u - t)}{u_m} B_{0m}(u) \right\}$$

$$\begin{aligned}
& + \frac{1}{r^2} \left[-2u_m [s_m(s-u) + 2m_e^2 t] C_{mmmm}(t) - 2stu_m C_{0mm}(s) - 2t(r^2 - m_e^2 u_m) C_{0mm}(u) \right. \\
& \quad - u_m [st(s+2u) + 4m_e^2 r^2 - 3m_e^4 t] [D_{m0mm}(t, s) + D_{m0mm}(t, u)] \\
& \quad \left. - t^2 u_m (s + m_e^2) D_{m0mm}(t, u) \right] \Big\}, \\
\mathcal{M}_1(++--) & = 4\alpha^2 \frac{m_e^3 \sqrt{-t}}{s_m^2} \left\{ -\frac{s_m}{m_e^2} + 2m_e^2 \frac{t}{u_m} B' + \frac{s + m_e^2}{s_m} B_{0m}(s) + s_m \frac{3u - m_e^2}{u_m^2} B_{0m}(u) \right. \\
& \quad - 2s_m [C_{mmmm}(t) + C_{0mm}(s) - C_{0mm}(u)] - s_m (2s + u_m) D_{m0mm}(t, s) \\
& \quad \left. - s_m (s + m_e^2) D_{m0mm}(t, u) \right\}. \tag{3.2}
\end{aligned}$$

The scalar integrals read explicitly

$$\begin{aligned}
B' & = \frac{\partial B_0}{\partial p^2}(p^2, m_e, \lambda) \Big|_{p^2=m_e^2} = -\frac{1}{m_e^2} \left[1 + \ln\left(\frac{\lambda}{m_e}\right) \right], \\
B_{mm}(t) & = B_0(t, m_e, m_e) - B_0(0, m_e, m_e) - 2 = \beta_t \ln(x_t), \\
B_{0m}(v) & = B_0(v, 0, m_e) - B_0(0, 0, m_e) - 1 = -\frac{v_m}{v} \ln\left(-\frac{v_m + i\epsilon}{m_e^2}\right), \\
C_{mmmm}(t) & = C_0(0, 0, t, m_e, m_e, m_e) = \frac{1}{2t} \ln^2(x_t), \\
C_{m0m}(t) & = C_0(m_e^2, m_e^2, t, m_e, \lambda, m_e) \\
& = \frac{1}{\beta_t t} \left[\ln\left(\frac{\lambda^2}{m_e^2}\right) \ln(x_t) + \frac{1}{2} \ln^2(x_t) + 2 \text{Li}_2(1+x_t) - \frac{\pi^2}{2} - 2\pi i \ln(1+x_t) \right], \\
C_{0mm}(v) & = C_0(m_e^2, 0, v, 0, m_e, m_e) \\
& = \frac{1}{v_m} \left[\text{Li}_2\left(-\frac{v_m + i\epsilon}{m_e^2}\right) + \ln\left(\frac{v + i\epsilon}{m_e^2}\right) \ln\left(-\frac{v_m + i\epsilon}{m_e^2}\right) \right], \\
D_{m0mm}(t, v) & = D_0(m_e^2, m_e^2, 0, 0, t, v, m_e, \lambda, m_e, m_e) \\
& = \frac{1}{\beta_t t v_m} \left[2 \ln(x_t) \ln\left(\frac{\lambda m_e}{-v_m - i\epsilon}\right) - 2 \text{Li}_2(1-x_t) \right. \\
& \quad \left. + 2 \text{Li}_2(1+x_t) - \frac{\pi^2}{2} - 2\pi i \ln(1+x_t) \right], \tag{3.3}
\end{aligned}$$

with the dilogarithm $\text{Li}_2(x) = -\int_0^1 dt \ln(1-xt)/t$ and

$$v_m = v - m_e^2, \quad \beta_t = \sqrt{1 - \frac{4m_e^2}{t + i\epsilon}}, \quad x_t = \frac{\beta_t - 1}{\beta_t + 1}. \tag{3.4}$$

In (3.3), λ denotes an infinitesimal photon mass, which is chosen as IR regulator and drops out after adding soft-bremsstrahlung corrections. The quantity $i\epsilon$ ($\epsilon > 0$) represents an infinitesimal imaginary part specifying on which side of the cut a multi-valued function has to be evaluated. The definition of the momentum-space integrals and of the arguments of the standard functions B_0 , C_0 , D_0 can be found in the appendix of Ref. [14].

As an additional check of our one-loop results, we have analytically compared the relative corrections $\mathcal{M}_1/\mathcal{M}_0$ with the corresponding results $f^{(4)}/f^{(2)}$ of Milton et al. [9]. Apart from a trivially missing global sign in Ref. [9] for the configuration $(-+++)$, which has also been pointed out by Swartz [12], we find complete agreement.

Finally, we consider the one-loop corrections to low-energy Compton scattering in more detail. As already mentioned in the introduction, the complete QED corrections to the cross sections vanish in the low-energy limit $\beta \rightarrow 0$ owing to Thirring's theorem [5,6]. Upon inspecting the amplitudes and the phase space for photon bremsstrahlung, one finds that all real $\mathcal{O}(\alpha)$ corrections vanish at least like β^2 relative to the Born cross section. Thus, only loop corrections contribute in order $\beta\alpha$ relative to the lowest-order cross section. We have explicitly expanded our results (3.2) for $\beta \rightarrow 0$ and get

$$\mathcal{M}_1 = [\delta_{\text{low}} + \mathcal{O}(\beta^2)\alpha] \mathcal{M}_0 \quad (3.5)$$

with the simple factors

$$\begin{aligned} \delta_{\text{low}}(\pm\pm\pm\pm) &= \frac{\alpha\beta}{\pi} \frac{\sin^2(\frac{\theta}{2})}{\cos^2(\frac{\theta}{2}) + \beta[2 - \cos^2(\frac{\theta}{2})]}, \\ \delta_{\text{low}}(\pm\mp\pm\mp) &= 0, \\ \delta_{\text{low}}(\pm\mp\mp\pm) &= \frac{\alpha\beta}{\pi}, \\ \delta_{\text{low}}(\pm\mp\mp\mp) &= \delta_{\text{low}}(\pm\pm\mp\pm) = -\frac{\alpha\beta}{2\pi}, \\ \delta_{\text{low}}(\pm\pm\pm\mp) &= \delta_{\text{low}}(\pm\mp\pm\pm) = \frac{\alpha\beta}{2\pi}, \\ \delta_{\text{low}}(\pm\pm\mp\mp) &= -\frac{\alpha\beta}{\pi} \sin^{-2}(\frac{\theta}{2}). \end{aligned} \quad (3.6)$$

In the denominator of $\delta_{\text{low}}(\pm\pm\pm\pm)$ we keep the term $\cos^2(\frac{\theta}{2}) + \beta[2 - \cos^2(\frac{\theta}{2})]$ exactly, in order to avoid a mismatch when the pole in θ is cancelled in the product $\delta_{\text{low}}\mathcal{M}_0$.

Using these expressions to calculate the corrected cross sections $\sigma(P_e, P_\gamma)$, and retaining only terms linear in β , we find

$$\frac{d\sigma(+1, \pm 1)}{d \cos \theta} = [1 + \delta_{\text{low}}^\pm + \mathcal{O}(\beta^2)\alpha] \frac{d\sigma_0(+1, \pm 1)}{d \cos \theta}, \quad \delta_{\text{low}}^\pm = \mp \frac{\alpha\beta}{\pi} \sin^2(\frac{\theta}{2}) \frac{1 - 3 \cos \theta}{1 + \cos^2 \theta}. \quad (3.7)$$

Owing to

$$\frac{d\sigma_0(+1, \pm 1)}{d \cos \theta} = \frac{\pi\alpha^2}{m_e^2} [1 + \cos^2 \theta + \mathcal{O}(\beta)], \quad (3.8)$$

this implies that there is no correction of order $\beta\alpha$ to the unpolarized cross section in the low-energy limit. From (3.8) we can also deduce that the lowest-order asymmetry $A_{\text{LR},0}$ vanishes like $\mathcal{O}(\beta)$. Thus, the relative correction δ_A to $A_{\text{LR},0}$ does not tend to zero for $\beta \rightarrow 0$, since the factors β in δ_{low}^\pm are cancelled by a factor β in $A_{\text{LR},0}$. Explicitly we get

$$A_{\text{LR}} = [1 + \delta_{A,\text{low}} + \mathcal{O}(\beta)\alpha] A_{\text{LR},0}, \quad \delta_{A,\text{low}} = \frac{\alpha}{\pi} \frac{3 \cos \theta - 1}{4(\beta + \cos \theta)}, \quad (3.9)$$

where again $\beta + \cos \theta$ in the denominator of $\delta_{A,\text{low}}$ was kept exactly, in order to account for the exact pole position in $A_{\text{LR},0}$. The approximation (3.9) is applicable to all asymmetries defined via differential cross sections that are linear distributions in $\cos \theta$. Since $d\bar{E}'_e = d\bar{E}'_\gamma = E_\gamma \gamma_b \beta_b d \cos \theta$ [see (2.13)], the approximation is, in particular, valid for distributions in \bar{E}'_e and \bar{E}'_γ . The analogous approximation for the correction to the asymmetry defined via total cross sections can be obtained in a similar way; the result is

$$\delta_{A,\text{low}} = \frac{3\alpha}{2\pi}. \quad (3.10)$$

4 Real corrections

4.1 Soft-photonic bremsstrahlung

Radiative corrections resulting from the emission of soft photons are proportional to the lowest-order cross section of the corresponding process. The calculation of the relative correction factor δ_{soft} in $\mathcal{O}(\alpha)$ is straightforward [16] and involves the integration over the phase space of the emitted photon, the energy of which is bounded by the small soft-photon cut ΔE . Note that δ_{soft} is frame-dependent owing to this condition. In the CM system the soft-photon correction factor is given by

$$\delta_{\text{soft}} = \frac{\alpha}{\pi} \left\{ \ln\left(\frac{\lambda^2}{4\Delta E^2}\right) + \frac{s + m_e^2}{s - m_e^2} \ln\left(\frac{s}{m_e^2}\right) + \frac{t - 2m_e^2}{\beta_t t} \left[\ln(x_t) \ln\left(\frac{\lambda^2}{4\Delta E^2}\right) - \frac{1}{2} \ln^2\left(\frac{s}{m_e^2}\right) - \text{Li}_2\left(1 - \frac{s}{m_e^2} x_t\right) - \text{Li}_2\left(1 - \frac{m_e^2}{s} x_t\right) + 2 \text{Re}\{\text{Li}_2(1 + x_t)\} - \frac{\pi^2}{2} \right] \right\}, \quad (4.1)$$

where the $\ln \lambda^2$ terms cancel against the corresponding IR-divergent contributions of the virtual corrections. In practice, λ can be set to any value providing a check of IR finiteness in the sum of virtual and soft-photonic corrections. The dependence on the soft-photon cut $\Delta E \ll E_\gamma$ drops out after adding the numerically integrated corrections induced by the process $e^- \gamma \rightarrow e^- \gamma \gamma$, where either emitted photon has an energy larger than ΔE .

4.2 Hard photon emission—the process $e^- \gamma \rightarrow e^- \gamma \gamma$

The emission of an additional photon with finite energy leads us to the kinematically different process

$$e^-(p, \sigma) + \gamma(k, \lambda) \longrightarrow e^-(p', \sigma') + \gamma(k'_1, \lambda'_1) + \gamma(k'_2, \lambda'_2). \quad (4.2)$$

The incoming momenta p, k and the polarization vectors of the incoming photon are the same as in Sect. 2. In the CM system the outgoing momenta p' and k'_n ($n = 1, 2$) are specified by

$$\begin{aligned} p'^\mu &= E'_e(1, \beta' \sin \theta'_e \cos \phi'_e, \beta' \sin \theta'_e \sin \phi'_e, \beta' \cos \theta'_e), & \beta' &= \sqrt{1 - m_e^2/E_e'^2}, \\ k_n'^\mu &= E'_{\gamma,n}(1, \sin \theta'_{\gamma,n} \cos \phi'_{\gamma,n}, \sin \theta'_{\gamma,n} \sin \phi'_{\gamma,n}, \cos \theta'_{\gamma,n}). \end{aligned} \quad (4.3)$$

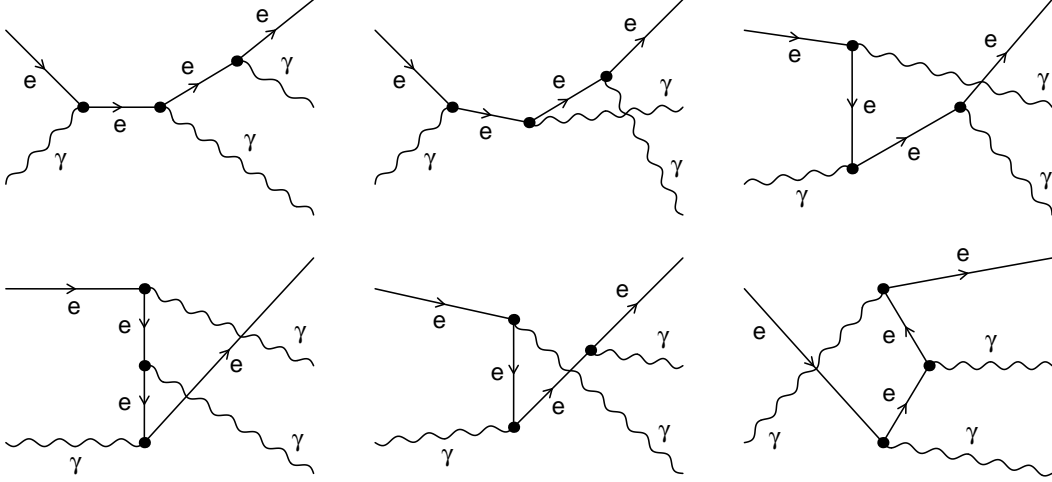


Figure 3: Tree diagrams for $e^- \gamma \rightarrow e^- \gamma \gamma$

The polarization vectors of the outgoing photons read

$$\begin{aligned} \varepsilon'^{\ast\mu}(k'_n, \lambda'_n = \pm 1) = \frac{e^{\pm i\phi'_{\gamma,n}}}{\sqrt{2}} & (0, -\cos\theta'_{\gamma,n} \cos\phi'_{\gamma,n} \mp i \sin\phi'_{\gamma,n}, \\ & -\cos\theta'_{\gamma,n} \sin\phi'_{\gamma,n} \pm i \cos\phi'_{\gamma,n}, \sin\theta'_{\gamma,n}). \end{aligned} \quad (4.4)$$

One of the angles $\phi'_{\gamma,n}$ or ϕ'_e can be put to zero upon orienting the coordinate system appropriately. The lowest-order cross section for $e^- \gamma \rightarrow e^- \gamma \gamma$, which yields an $\mathcal{O}(\alpha)$ correction to the Compton process, is given by

$$\sigma_\gamma(P_e, P_\gamma) = \frac{1}{4E_\gamma \sqrt{s}} \int d\Gamma_\gamma \sum_{\sigma, \lambda, \sigma', \lambda'_1, \lambda'_2} \frac{1}{8} (1 + 2\sigma P_e)(1 + \lambda P_\gamma) |\mathcal{M}_\gamma(\sigma, \lambda, \sigma', \lambda'_1, \lambda'_2)|^2, \quad (4.5)$$

where the phase-space integral is defined by

$$\int d\Gamma_\gamma = \int \frac{d^3\mathbf{p}'}{(2\pi)^3 2E'_e} \int \frac{d^3\mathbf{k}'_1}{(2\pi)^3 2E'_{\gamma,1}} \int \frac{d^3\mathbf{k}'_2}{(2\pi)^3 2E'_{\gamma,2}} (2\pi)^4 \delta(p + k - p' - k'_1 - k'_2). \quad (4.6)$$

Since we sum over all polarizations in the final state and integrate over the full three-particle phase space, we have included a factor 1/2 in (4.5), in order to compensate for double counting of identical configurations of the photons. The phase-space integration is performed numerically by Vegas [22].

The helicity amplitudes \mathcal{M}_γ , which receive contributions from the six diagrams shown in Fig. 3, have been calculated in three independent ways, the results of which are in complete mutual numerical agreement. One calculation is based on the spinor calculus described in Ref. [23]; the second one makes use of an explicit representation of spinors, polarization vectors, and Dirac matrices. In the following we present the result of the third calculation, which has been performed using the Weyl–van-der-Waerden (WvdW) formalism. An introduction into this formalism and more details can be found in Ref. [15]. In particular, the explicit form of the electron spinors, which is needed for the transition

to transversely polarized electrons, can be found there. Here we give only the ingredients that are necessary for the evaluation of the helicity amplitudes.

In the WvdW formalism, spinor chains and Minkowski inner products are expressed in terms of antisymmetric spinor products

$$\langle \psi \phi \rangle = -\langle \phi \psi \rangle = \psi_1 \phi_2 - \psi_2 \phi_1 \quad (4.7)$$

of two-component WvdW spinors ψ_A, ϕ_A . For each light-like momentum there is an associated momentum spinor. Specifically, we have the spinors

$$k_A = \sqrt{2E_\gamma} \begin{pmatrix} 0 \\ 1 \end{pmatrix}, \quad k'_{n,A} = \sqrt{2E'_{\gamma,n}} \begin{pmatrix} e^{-i\phi'_{\gamma,n}} \cos \frac{\theta'_{\gamma,n}}{2} \\ \sin \frac{\theta'_{\gamma,n}}{2} \end{pmatrix}, \quad n = 1, 2, \quad (4.8)$$

for the photon momenta k and k'_n ($n = 1, 2$). For each time-like momentum there are two associated WvdW spinors; for p we have

$$\kappa_{1,A} = \sqrt{E_e(1+\beta)} \begin{pmatrix} 1 \\ 0 \end{pmatrix}, \quad \kappa_{2,A} = \frac{m_e}{\sqrt{E_e(1+\beta)}} \begin{pmatrix} 0 \\ -1 \end{pmatrix}, \quad (4.9)$$

and for p'

$$\kappa'_{1,A} = \sqrt{E'_e(1+\beta')} \begin{pmatrix} e^{-i\phi'_e} \cos \frac{\theta'_e}{2} \\ \sin \frac{\theta'_e}{2} \end{pmatrix}, \quad \kappa'_{2,A} = \frac{m_e}{\sqrt{E'_e(1+\beta')}} \begin{pmatrix} \sin \frac{\theta'_e}{2} \\ -e^{+i\phi'_e} \cos \frac{\theta'_e}{2} \end{pmatrix}. \quad (4.10)$$

We note that $\langle \kappa_2 \kappa_1 \rangle = \langle \kappa'_2 \kappa'_1 \rangle = m_e$. The different helicity amplitudes for $e^- \gamma \rightarrow e^- \gamma \gamma$ can be completely expressed in terms of spinor products of the WvdW spinors $k_A, k'_{1,A}, k'_{2,A}, \kappa_{1,A}, \kappa_{2,A}, \kappa'_{1,A}, \kappa'_{2,A}$. However, at some places it is convenient to keep the usual Minkowski inner products like $p \cdot k = p_\mu k^\mu$, etc. Moreover, we introduce the following abbreviations:

$$\begin{aligned} \langle a P b \rangle &= \sum_{i=1,2} \langle a \kappa_i \rangle^* \langle b \kappa_i \rangle, \\ \langle a P P' a \rangle &= \sum_{i,j=1,2} \langle a \kappa_i \rangle^* \langle \kappa'_j \kappa_i \rangle \langle \kappa'_j a \rangle^*, \quad a, b = k, k'_1, k'_2. \end{aligned} \quad (4.11)$$

The presentation of the amplitudes can be shortened by exploiting discrete symmetries. Helicity amplitudes with opposite helicity configurations are related by parity, leading to¹

$$\mathcal{M}_\gamma(-\sigma, -\lambda, -\sigma', -\lambda'_1, -\lambda'_2) = \text{sgn}(\sigma\sigma') \mathcal{M}_\gamma(\sigma, \lambda, \sigma', \lambda'_1, \lambda'_2)^*, \quad (4.12)$$

and the two outgoing photons can be interchanged owing to Bose symmetry,

$$\mathcal{M}_\gamma(\sigma, \lambda, \sigma', \lambda'_2, \lambda'_1) = \mathcal{M}_\gamma(\sigma, \lambda, \sigma', \lambda'_1, \lambda'_2) \Big|_{k'_1 \leftrightarrow k'_2}. \quad (4.13)$$

¹The global signs in (4.12) and in similar relations below are convention-dependent. We consequently stick to the conventions of Ref. [15].

Making use of these relations, we get three independent amplitudes for fixed electron helicities:

$$\mathcal{M}_\gamma(\sigma, \lambda, \sigma', \lambda'_1, \lambda'_2) = \frac{e^3 A_{\lambda\lambda'_1\lambda'_2}(\sigma, \sigma')}{4\sqrt{2}(p \cdot k)(p \cdot k'_1)(p \cdot k'_2)}, \quad (4.14)$$

where

$$\begin{aligned} A_{+++}(\sigma, \sigma') &= m_e \frac{(\langle k'_1 k'_2 \rangle^*)^2}{2(p' \cdot k)} \left(-\langle k P P' k \rangle^* \langle \phi \psi' \rangle + 2(p \cdot k) \langle k \psi' \rangle \langle k \phi \rangle \right) \\ &\quad - \frac{\langle k'_2 P k \rangle}{(p' \cdot k'_1)} \left[\langle k'_1 P P' k'_1 \rangle (\langle k'_2 \psi \rangle^* \langle k \psi' \rangle + \langle k'_2 \phi \rangle^* \langle k \phi \rangle) \right. \\ &\quad \left. + 2(p \cdot k'_1) \langle k \phi \rangle \langle k'_1 \phi' \rangle^* \langle k'_1 k'_2 \rangle^* \right] + (k'_1 \leftrightarrow k'_2), \\ A_{-++}(\sigma, \sigma') &= m_e \langle \phi \psi' \rangle \left[\frac{(\langle k'_2 k \rangle^*)^2}{(p' \cdot k'_1)} \langle k'_1 P P' k'_1 \rangle - \frac{(\langle k'_1 k'_2 \rangle^*)^2}{2(p' \cdot k)} \langle k P P' k \rangle \right] + (k'_1 \leftrightarrow k'_2), \\ A_{--+}(\sigma, \sigma') &= m_e \frac{(\langle k'_2 k \rangle^*)^2}{(p' \cdot k'_1)} \left(\langle k'_1 P P' k'_1 \rangle^* \langle \phi \psi' \rangle + 2(p \cdot k'_1) \langle k'_1 \psi' \rangle \langle k'_1 \phi \rangle \right) \\ &\quad - \frac{\langle k P k'_1 \rangle}{(p' \cdot k'_2)} \left[\langle k'_2 P P' k'_2 \rangle (\langle k \psi \rangle^* \langle k'_1 \psi' \rangle + \langle k \phi \rangle^* \langle k'_1 \phi \rangle) \right. \\ &\quad \left. + 2(p \cdot k'_2) \langle k'_1 \phi \rangle \langle k'_2 \phi' \rangle^* \langle k'_2 k \rangle^* \right] \\ &\quad + \frac{\langle k'_2 P k'_1 \rangle}{(p' \cdot k)} \left[\langle k P P' k \rangle (\langle k'_2 \psi \rangle^* \langle k'_1 \psi' \rangle + \langle k'_2 \phi \rangle^* \langle k'_1 \phi \rangle) \right. \\ &\quad \left. + 2(p \cdot k) \langle k'_1 \phi \rangle \langle k \phi' \rangle^* \langle k'_2 k \rangle^* \right]. \end{aligned} \quad (4.15)$$

The auxiliary spinors ϕ , ψ , ϕ' , ψ' contain the information about the electron helicity configurations (σ, σ') . Their actual insertions are

$$(\phi, \psi) = \begin{cases} (\kappa_1, -\kappa_2) & \text{for } \sigma = +, \\ (\kappa_2, \kappa_1) & \text{for } \sigma = -, \end{cases} \quad (\phi', \psi') = \begin{cases} (\kappa'_1, -\kappa'_2) & \text{for } \sigma' = +, \\ (\kappa'_2, \kappa'_1) & \text{for } \sigma' = -. \end{cases} \quad (4.16)$$

Actually, the quantity A_{--+} is related to A_{+++} via crossing symmetry for the photons $\gamma(k, \lambda)$ and $\gamma(k'_1, \lambda'_1)$, leaving only two independent amplitudes.

4.3 Associated pair creation—the process $e^- \gamma \rightarrow e^- e^- e^+$

If only electrons are detected in the final state, the reaction

$$e^-(p, \sigma) + \gamma(k, \lambda) \longrightarrow e^-(p'_1, \sigma'_1) + e^-(p'_2, \sigma'_2) + e^+(q, \tau) \quad (4.17)$$

represents an additional background process. The incoming momenta p and k are again the same as in Sect. 2. In the CM system the outgoing momenta p'_n ($n = 1, 2$) and q are specified by

$$\begin{aligned} p'_n{}^\mu &= E'_{e,n} (1, \beta'_{e,n} \sin \theta'_{e,n} \cos \phi'_{e,n}, \beta'_{e,n} \sin \theta'_{e,n} \sin \phi'_{e,n}, \beta'_{e,n} \cos \theta'_{e,n}), \\ q^\mu &= E_+(1, \beta_+ \sin \theta_+ \cos \phi_+, \beta_+ \sin \theta_+ \sin \phi_+, \beta_+ \cos \theta_+), \end{aligned} \quad (4.18)$$

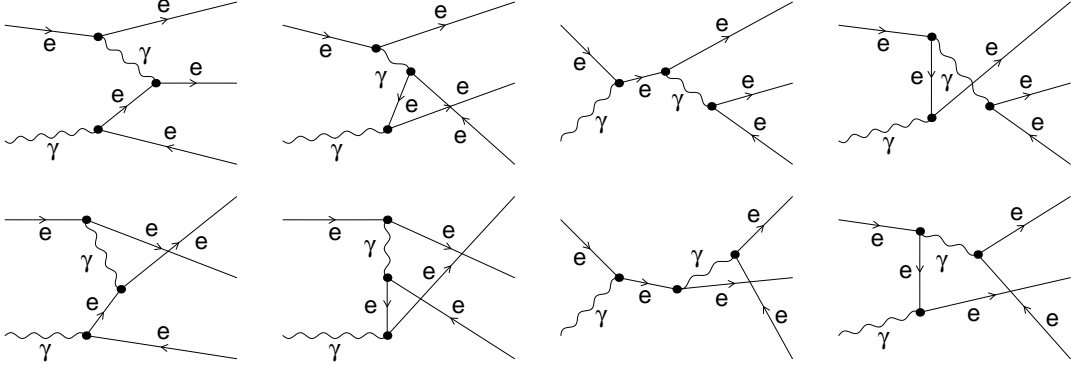


Figure 4: Tree diagrams for $e^- \gamma \rightarrow e^- e^- e^+$

with $\beta'_{e,n} = \sqrt{1 - m_e^2/E_{e,n}^2}$ and $\beta_+ = \sqrt{1 - m_e^2/E_+^2}$. The lowest-order cross section for $e^- \gamma \rightarrow e^- e^- e^+$ is obtained as

$$\sigma_e(P_e, P_\gamma) = \frac{1}{4E_\gamma \sqrt{s}} \int d\Gamma_e \sum_{\sigma, \lambda, \sigma'_1, \sigma'_2, \tau} \frac{1}{8} (1 + 2\sigma P_e)(1 + \lambda P_\gamma) |\mathcal{M}_e(\sigma, \lambda, \sigma'_1, \sigma'_2, \tau)|^2, \quad (4.19)$$

where the phase-space integral reads

$$\int d\Gamma_e = \int \frac{d^3 \mathbf{p}'_1}{(2\pi)^3 2E'_{e,1}} \int \frac{d^3 \mathbf{p}'_2}{(2\pi)^3 2E'_{e,2}} \int \frac{d^3 \mathbf{q}}{(2\pi)^3 2E_+} (2\pi)^4 \delta(p + k - p'_1 - p'_2 - q). \quad (4.20)$$

Double counting of identical configurations of the electrons in the final state is avoided by including a factor 1/2 in (4.19). The phase-space integration is again performed numerically by Vegas [22].

The eight diagrams shown in Fig. 4 contribute to the helicity amplitudes \mathcal{M}_e in lowest order. The amplitudes \mathcal{M}_e have been calculated in the WvdW formalism as well as by using explicit spinors, polarization vectors, and Dirac matrices. Here we again present the result in terms of WvdW spinor products, as in the previous section for $e^- \gamma \rightarrow e^- \gamma \gamma$. The spinors $\kappa_{i,A}$ ($i = 1, 2$) and k_A for the incoming momenta p and k , are defined in (4.8) and (4.9), respectively. For the outgoing momenta p'_n ($n = 1, 2$) and q we introduce the following spinors:

$$\begin{aligned} \kappa'_{n1,A} &= \sqrt{E'_{e,n}(1 + \beta'_{e,n})} \begin{pmatrix} e^{-i\phi'_{e,n}} \cos \frac{\theta'_{e,n}}{2} \\ \sin \frac{\theta'_{e,n}}{2} \end{pmatrix}, & \kappa'_{n2,A} &= \frac{m_e}{\sqrt{E'_{e,n}(1 + \beta'_{e,n})}} \begin{pmatrix} \sin \frac{\theta'_{e,n}}{2} \\ -e^{+i\phi'_{e,n}} \cos \frac{\theta'_{e,n}}{2} \end{pmatrix}, \\ \rho_{1,A} &= \sqrt{E_+(1 + \beta_+)} \begin{pmatrix} e^{-i\phi_+} \cos \frac{\theta_+}{2} \\ \sin \frac{\theta_+}{2} \end{pmatrix}, & \rho_{2,A} &= \frac{m_e}{\sqrt{E_+(1 + \beta_+)}} \begin{pmatrix} \sin \frac{\theta_+}{2} \\ -e^{+i\phi_+} \cos \frac{\theta_+}{2} \end{pmatrix}. \end{aligned} \quad (4.21)$$

We note that $\langle \kappa'_{12} \kappa'_{11} \rangle = \langle \kappa'_{22} \kappa'_{21} \rangle = \langle \rho_2 \rho_1 \rangle = m_e$. In analogy to (4.11) we define

$$\begin{aligned} \langle k P P'_n k \rangle &= \sum_{i,j=1,2} \langle k \kappa_i \rangle^* \langle \kappa'_{nj} \kappa_i \rangle \langle \kappa'_{nj} k \rangle^*, \\ \langle k Q P'_n k \rangle &= \sum_{i,j=1,2} \langle k \rho_i \rangle^* \langle \kappa'_{nj} \rho_i \rangle \langle \kappa'_{nj} k \rangle^*, \quad n = 1, 2. \end{aligned} \quad (4.22)$$

Helicity amplitudes with opposite helicity configurations are related by parity, yielding

$$\mathcal{M}_e(-\sigma, -\lambda, -\sigma'_1, -\sigma'_2, -\tau) = -\text{sgn}(\sigma\sigma'_1\sigma'_2\tau)\mathcal{M}_e(\sigma, \lambda, \sigma'_1, \sigma'_2, \tau)^*, \quad (4.23)$$

and the amplitudes are antisymmetric with respect to the interchange of the two outgoing electrons:

$$\mathcal{M}_e(\sigma, \lambda, \sigma'_2, \sigma'_1, \tau) = -\mathcal{M}_e(\sigma, \lambda, \sigma'_1, \sigma'_2, \tau)\Big|_{p'_1 \leftrightarrow p'_2}. \quad (4.24)$$

The actual calculation of the helicity amplitudes is most conveniently performed by first considering the process $e^- \gamma \rightarrow e^- f \bar{f}$ with $f \neq e^-$, where only four diagrams contribute instead of eight. The amplitudes for $e^- \gamma \rightarrow e^- e^- e^+$ are obtained from these intermediate results by first antisymmetrizing the amplitudes with respect to the fields e^- and f in the final state, and then setting $f = e^-$. Using (4.23), all helicity amplitudes

$$\mathcal{M}_e(\sigma, \lambda, \sigma'_1, \sigma'_2, \tau) = -\frac{e^3}{\sqrt{2}} \left[A_\lambda(\sigma, \sigma'_1, \sigma'_2, \tau) - A_\lambda(\sigma, \sigma'_2, \sigma'_1, \tau) \Big|_{p'_1 \leftrightarrow p'_2, \phi'_1 \leftrightarrow \phi'_2, \psi'_1 \leftrightarrow \psi'_2} \right] \quad (4.25)$$

can be deduced from one generic function

$$\begin{aligned} A_+(\sigma, \sigma'_1, \sigma'_2, \tau) = & \left\{ \frac{\langle kQP'_2k \rangle^*}{2(p'_2 \cdot k)(q \cdot k)[m_e^2 - (p \cdot p'_1)]} + \frac{\langle kPP'_1k \rangle^*}{2(p \cdot k)(p'_1 \cdot k)[m_e^2 + (p'_2 \cdot q)]} \right\} \\ & \times \left(\langle \psi\phi'_2 \rangle^* \langle \psi'_1\xi \rangle + \langle \psi\eta \rangle^* \langle \psi'_1\psi'_2 \rangle + \langle \phi'_1\phi'_2 \rangle^* \langle \phi\xi \rangle + \langle \phi'_1\eta \rangle^* \langle \phi\psi'_2 \rangle \right) \\ & + \frac{1}{m_e^2 - (p \cdot p'_1)} \left[\frac{\langle k\xi \rangle}{(q \cdot k)} \left(\langle k\psi'_1 \rangle \langle \psi\phi'_2 \rangle^* + \langle k\phi \rangle \langle \phi'_1\phi'_2 \rangle^* \right) \right. \\ & \quad \left. - \frac{\langle k\psi'_2 \rangle}{(p'_2 \cdot k)} \left(\langle k\psi'_1 \rangle \langle \psi\eta \rangle^* + \langle k\phi \rangle \langle \phi'_1\eta \rangle^* \right) \right] \\ & + \frac{1}{m_e^2 + (p'_2 \cdot q)} \left[\frac{\langle k\psi'_1 \rangle}{(p'_1 \cdot k)} \left(\langle k\xi \rangle \langle \psi\phi'_2 \rangle^* + \langle k\psi'_2 \rangle \langle \psi\eta \rangle^* \right) \right. \\ & \quad \left. + \frac{\langle k\phi \rangle}{(p \cdot k)} \left(\langle k\xi \rangle \langle \phi'_1\phi'_2 \rangle^* + \langle k\psi'_2 \rangle \langle \phi'_1\eta \rangle^* \right) \right], \quad (4.26) \end{aligned}$$

where the spinors ϕ, ψ are the same as in (4.16), and $\phi'_n, \psi'_n, \xi, \eta$ ($n = 1, 2$) are given by

$$(\phi'_n, \psi'_n) = \begin{cases} (\kappa'_{n1}, -\kappa'_{n2}) & \text{for } \sigma'_n = +, \\ (\kappa'_{n2}, \kappa'_{n1}) & \text{for } \sigma'_n = -, \end{cases} \quad (\xi, \eta) = \begin{cases} (-\rho_2, \rho_1) & \text{for } \tau = +, \\ (\rho_1, \rho_2) & \text{for } \tau = -. \end{cases} \quad (4.27)$$

The amplitude $A_+(\sigma, \sigma'_1, \sigma'_2, \tau)$ is composed of two gauge-invariant contributions, one of them consists of all the terms involving the denominator $m_e^2 - (p \cdot p'_1)$, the other consists of the terms with the denominator $m_e^2 + (p'_2 \cdot q)$. The two gauge-invariant contributions correspond to the first two pairs of graphs in Fig. 4 and are related to each other by appropriately interchanging the external fermions.

5 Numerical results

In this section we apply our analytical results to various cases of physical relevance. We focus on polarimeters that determine the polarization of electron beams by measuring the

asymmetry (2.18). The cross sections entering this asymmetry are measured by either detecting the scattered electron or the scattered photon. We consider, in particular, the polarimeters for CEBAF, for the SLC, and for an e^+e^- collider with beam energies of 500 GeV.

For the numerical evaluation we use

$$\alpha^{-1} = 137.0359895, \quad m_e = 0.51099906 \text{ MeV}. \quad (5.1)$$

5.1 Results for the CEBAF polarimeter

As a first application we discuss the CEBAF polarimeter [2]. Here an electron beam with an energy of a few GeV collides with a laser beam of a few eV. We consider three setups:

\bar{E}_γ [eV]	\bar{E}_e [GeV]	E_{CM} [MeV]	$\bar{E}'_{\gamma,\text{max}}$ [GeV]	β	$\gamma_b/10^3$
1.165	4.0	0.5289	0.2665	0.03446	7.563
1.165	6.0	0.5377	0.5803	0.05082	11.16
1.165	8.0	0.5463	0.9995	0.06663	14.65

(5.2)

The backward-scattered photons are detected by a calorimeter that is located roughly 5 m after the interaction point perpendicular to the incident electron with transverse extension of $10 \text{ cm} \times 10 \text{ cm}$. If two photons (from double Compton scattering events) hit the detector, only the sum of their energies is detected.

We have implemented the detector in our calculation. The hard-photon part of the differential cross section $d\sigma/d\bar{E}'_\gamma$ is obtained as the sum of the cross section where two photons hit the detector with $\bar{E}'_\gamma = \bar{E}'_{\gamma,1} + \bar{E}'_{\gamma,2}$ and the cross sections where exactly one photon hits the detector with $\bar{E}'_\gamma = \bar{E}'_{\gamma,1}$ or $\bar{E}'_\gamma = \bar{E}'_{\gamma,2}$. Since the final-state photons are strongly boosted in the backward direction, almost all photons hit the detector. Numerically our results with and without detector cuts practically coincide, i.e. the finite extension of the detector turns out to be irrelevant.

In Tables 1, 2 and in Figs. 5, 6 we show the unpolarized lowest-order cross section $d\sigma_0/d\bar{E}'_\gamma$ and the lowest-order asymmetry $A_{\text{LR},0}$ as a function of the photon energy \bar{E}'_γ deposited in the calorimeter. In addition, we show the corrections to these quantities.

The relative corrections δ to the unpolarized cross section, defined by

$$\frac{d\sigma}{d\bar{E}'_\gamma} = \frac{d\sigma_0}{d\bar{E}'_\gamma} (1 + \delta), \quad (5.3)$$

are below roughly 10^{-4} , take their largest values for small photon energies and decrease with increasing photon energy. The smallness of these corrections can be explained by the suppression with a factor $\beta^2 \lesssim 4 \times 10^{-3}$ (see Sect. 3). The absolute corrections ΔA_{LR} to the asymmetry reach at most few 10^{-4} for large photon energies and roughly follow the shape of the lowest-order asymmetries. The relative corrections δ_A to A_{LR} , defined by

$$A_{\text{LR}} = A_{\text{LR},0} (1 + \delta_A), \quad (5.4)$$

\bar{E}'_γ [GeV]	$\frac{d\sigma_0}{d\bar{E}'_\gamma}$ [mb/GeV]	δ [%]	$A_{LR,0}$	$\Delta A_{LR} \times 100$	δ_A [%]	$\delta_{A,low}$ [%]
0.010	3258.0	0.0038	-0.0025	-0.0001	0.05	0.11
0.035	2737.5	0.0037	-0.0084	-0.0007	0.08	0.09
0.060	2322.2	0.0035	-0.0130	-0.0008	0.06	0.06
0.085	2016.3	0.0033	-0.0146	-0.0003	0.02	0.01
0.110	1824.1	0.0030	-0.0111	0.0012	-0.10	-0.13
0.135	1750.2	0.0025	-0.0015	0.0036	-2.48	-2.82
0.160	1799.2	0.0021	0.0133	0.0068	0.51	0.56
0.185	1976.0	0.0017	0.0300	0.0099	0.33	0.36
0.210	2285.7	0.0013	0.0456	0.0126	0.28	0.29
0.235	2733.4	0.0009	0.0580	0.0144	0.25	0.26
0.260	3324.7	-0.0003	0.0670	0.0156	0.23	0.24

Table 1: Lowest-order unpolarized cross section and asymmetry together with the corresponding corrections for the CEBAF polarimeter ($\bar{E}_e = 4$ GeV, $\bar{E}_\gamma = 1.165$ eV)

\bar{E}'_γ [GeV]	$\frac{d\sigma_0}{d\bar{E}'_\gamma}$ [mb/GeV]	δ [%]	$A_{LR,0}$	$\Delta A_{LR} \times 100$	δ_A [%]	$\delta_{A,low}$ [%]
0.010	858.50	0.0111	-0.0013	0.0007	-0.52	0.11
0.100	732.56	0.0107	-0.0123	-0.0005	0.04	0.09
0.200	616.50	0.0103	-0.0230	-0.0012	0.05	0.07
0.300	527.60	0.0098	-0.0288	-0.0008	0.03	0.02
0.400	468.14	0.0091	-0.0252	0.0013	-0.05	-0.09
0.500	440.57	0.0080	-0.0085	0.0057	-0.67	-0.88
0.600	447.56	0.0068	0.0207	0.0118	0.57	0.69
0.700	491.99	0.0057	0.0559	0.0183	0.33	0.38
0.800	576.99	0.0046	0.0889	0.0238	0.27	0.30
0.900	705.95	0.0029	0.1149	0.0277	0.24	0.27
0.990	862.64	-0.0036	0.1313	0.0298	0.23	0.25

Table 2: Lowest-order unpolarized cross section and asymmetry together with the corresponding corrections for the CEBAF polarimeter ($\bar{E}_e = 8$ GeV, $\bar{E}_\gamma = 1.165$ eV)

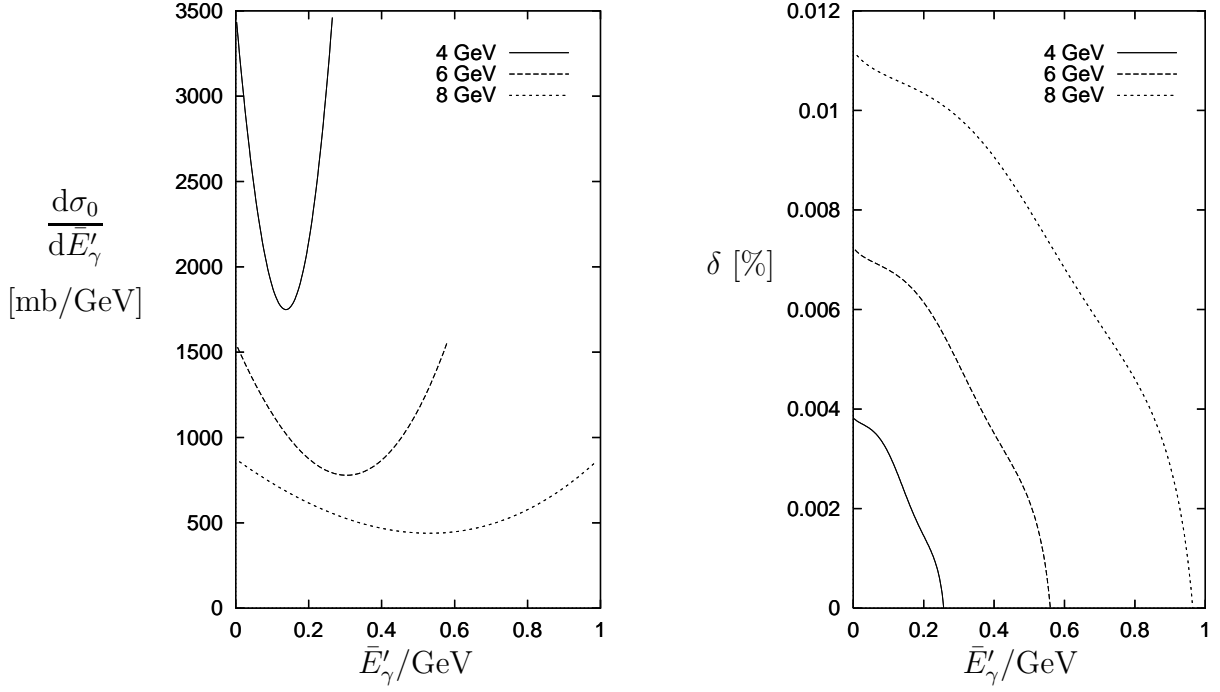


Figure 5: Lowest-order unpolarized cross section (left) and corresponding percentage relative corrections (right) for the CEBAF polarimeter ($\bar{E}_\gamma = 1.165$ eV)

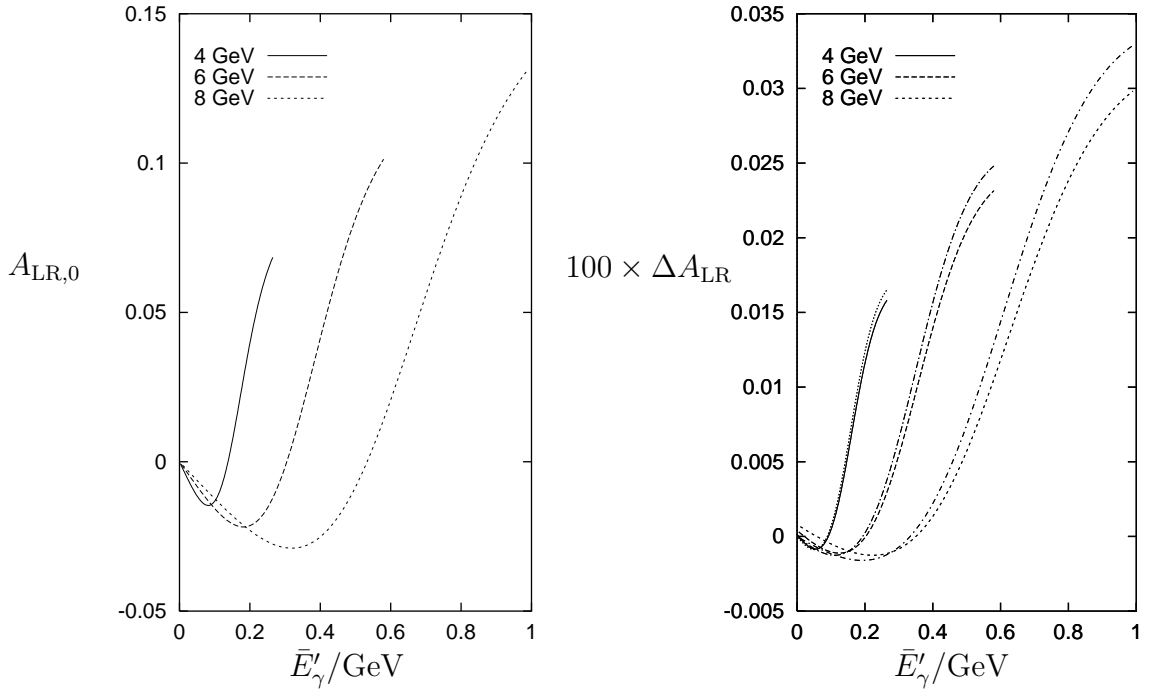


Figure 6: Lowest-order left-right asymmetry (left) and corresponding absolute corrections (right) for the CEBAF polarimeter ($\bar{E}_\gamma = 1.165$ eV). In the right plot, the lines next to the labelled ones correspond to the respective low-energy approximation.

\bar{E}_γ [GeV]	\bar{E}_e [GeV]	σ_0 [mb]	δ [%]	$A_{\text{LR},0}$	$\Delta A_{\text{LR}} \times 100$	δ_A [%]	$\delta_{A,\text{low}}$ [%]
1.165	4.0	621.80	0.0023	0.0160	0.0057	0.35	0.35
1.165	6.0	602.74	0.0045	0.0228	0.0082	0.36	0.35
1.165	8.0	585.17	0.0071	0.0289	0.0104	0.36	0.35

Table 3: Integrated lowest-order unpolarized cross section and left–right asymmetry together with the corresponding corrections for the CEBAF polarimeter

are of the expected order $\alpha/\pi \sim 2 \times 10^{-3}$, as long as the lowest-order asymmetry is not suppressed. Note that the low-energy approximation $\delta_{A,\text{low}}$ for δ_A , which is given in (3.9), works very well for CEBAF energies, where $\beta < 0.07$.

The total cross sections and the related asymmetries are listed together with the corresponding corrections in Table 3. The corresponding low-energy approximation $\delta_{A,\text{low}}$ is given in (3.10). If detector cuts on the outgoing photons are applied, the distribution $d\sigma/d\bar{E}'_\gamma$ becomes IR-singular for $\bar{E}'_\gamma \rightarrow 0$. For a well-defined total cross section σ , either a lower cut ΔE_γ for \bar{E}'_γ has to be introduced, or the detector cuts have to be dropped; the latter was done for Table 3.

In conclusion, the relative corrections to the polarization asymmetry measured at CEBAF are typically $\lesssim 0.4\%$, whenever the asymmetry is sizeable. For a polarization measurement at the 1% level the simple low-energy approximation is therefore fully sufficient.

5.2 Results for the SLD polarimeter

Next we consider the SLD polarimeter [1]. In this case an electron beam of about 45 GeV collides with a 2.33 eV photon beam. The scattered electrons are detected, and their energy is measured. Since we are going to perform a direct comparison of our results to the ones of Veltman [11] and Swartz [12], we take the input values

$$\bar{E}_\gamma = 2.34 \text{ eV}, \quad \bar{E}_e = 50 \text{ GeV}, \quad (5.5)$$

leading to

$$E_{\text{CM}} = 0.8539 \text{ MeV}, \quad \bar{E}'_{e,\text{min}} = 17.91 \text{ GeV}, \quad \beta = 0.4726, \quad \gamma_b = 5.856 \times 10^4. \quad (5.6)$$

As for the CEBAF detector, the finite extension of the detector is irrelevant because of the even stronger boost from the LAB system to the CM system.

In Table 4 we show the lowest-order cross section $d\sigma_0/d\bar{E}'_e$ and the asymmetry defined in (2.18) as a function of the energy of the scattered electron \bar{E}'_e together with the corresponding corrections. For SLC energies, the corrections to the cross section are no longer suppressed by β and are of the expected order $\alpha/\pi \sim 2 \times 10^{-3}$. The numerical analysis shows that the low-energy approximation (3.9) becomes useless and it is thus not given in the table.

\bar{E}'_e [GeV]	$\frac{d\sigma_0}{d\bar{E}'_e}$ [mb/GeV]	δ [%]	$A_{\text{LR},0}$	$\Delta A_{\text{LR}} \times 100$	δ_A [%]
17.92	17.504	-0.63	0.7717	0.0725	0.09
19.90	13.272	0.10	0.6102	0.0572	0.09
21.90	10.621	0.16	0.4177	0.0478	0.11
23.90	9.008	0.18	0.2181	0.0383	0.18
25.90	8.073	0.18	0.0374	0.0293	0.78
27.90	7.592	0.17	-0.1051	0.0226	-0.22
29.90	7.420	0.17	-0.2014	0.0195	-0.10
31.90	7.461	0.16	-0.2544	0.0199	-0.08
33.90	7.649	0.16	-0.2726	0.0232	-0.09
35.90	7.941	0.15	-0.2657	0.0284	-0.11
37.90	8.305	0.15	-0.2422	0.0347	-0.14
39.90	8.719	0.15	-0.2085	0.0418	-0.20
41.90	9.167	0.15	-0.1693	0.0492	-0.29
43.90	9.637	0.16	-0.1274	0.0568	-0.45
45.90	10.122	0.17	-0.0848	0.0645	-0.76
47.90	10.614	0.19	-0.0428	0.0723	-1.69
49.90	11.111	0.22	-0.0020	0.0801	-40.0

Table 4: Lowest-order unpolarized cross section and asymmetry together with the corresponding corrections for the SLD polarimeter ($\bar{E}_e = 50$ GeV, $\bar{E}_\gamma = 2.34$ eV)

The results for the total unpolarized cross section are

$$\sigma_0 = 299.89 \text{ mb}, \quad \delta = 0.14\%, \quad (5.7)$$

and for the related asymmetry we get

$$A_{\text{LR},0} = 0.03089, \quad \Delta A_{\text{LR}} = 0.00031, \quad \delta_A = 1.0\%. \quad (5.8)$$

In Figs. 7 and 8 we compare our results for the corrections to the unpolarized cross section and the asymmetry with the results of Swartz [12], which we directly obtained from the author, and Veltman, which are taken from Ref. [11]. For the corrections to the cross section, where the results of Swartz and Veltman disagree, we reproduce the results of Swartz well. For the asymmetry we confirm the results of Swartz who has found small deviations from Veltman.

As pointed out by Swartz, the inclusion of the $\mathcal{O}(\alpha)$ corrections increases the measured value of A_{LR} by 0.1%, since the polarization is determined using only scattered electrons with energies $\lesssim 20 \text{ GeV}$. This effect is too small and has the wrong sign to account for the discrepancy [24] in the experimental results for the effective leptonic weak mixing angle between SLC and LEP.

5.3 Results for an NLC polarimeter

Finally, we consider a polarimeter for a NLC. We assume an ‘‘SLD-like’’ polarimeter with the parameters

$$\bar{E}_\gamma = 2.33 \text{ eV}, \quad \bar{E}_e = 500 \text{ GeV}, \quad (5.9)$$

leading to

$$E_{\text{CM}} = 2.218 \text{ MeV}, \quad \bar{E}'_{e,\text{min}} = 26.53 \text{ GeV}, \quad \beta = 0.8992, \quad \gamma_b = 2.254 \times 10^5. \quad (5.10)$$

In this case we are at the onset of the relativistic regime, where because of enhanced logarithms the relative corrections start to exceed the naive expectation of the order $\alpha/\pi \sim 2 \times 10^{-3}$. Moreover, in addition to the bremsstrahlung process $e^- \gamma \rightarrow e^- \gamma \gamma$, also the associated pair-production process $e^- \gamma \rightarrow e^- e^- e^+$ contributes in the energy region

$$\bar{E}'_{e,\text{min}} = 34.36 \text{ GeV} < \bar{E}'_e < \bar{E}'_{e,\text{max}} = 386.05 \text{ GeV}. \quad (5.11)$$

We assume that both of the final-state electrons contribute separately to the electron-energy distribution, i.e. that they can be separated in the final state.

Our results for the lowest-order cross section $d\sigma/d\bar{E}'_e$ and the asymmetry, together with the corresponding relative corrections, are shown in Tables 5 and 6 as a function of the electron energy \bar{E}'_e . We separately give the relative corrections δ_1 to the cross sections of $e^- \gamma \rightarrow e^- \gamma(\gamma)$, defined by

$$\frac{d\sigma_1}{d\bar{E}'_e} = \frac{d\sigma_0}{d\bar{E}'_e} (1 + \delta_1), \quad (5.12)$$

and the corrections δ_e to the cross sections resulting from the process $e^- \gamma \rightarrow e^- e^- e^+$:

$$\frac{d\sigma_e}{d\bar{E}'_e} = \frac{d\sigma_0}{d\bar{E}'_e} \delta_e. \quad (5.13)$$

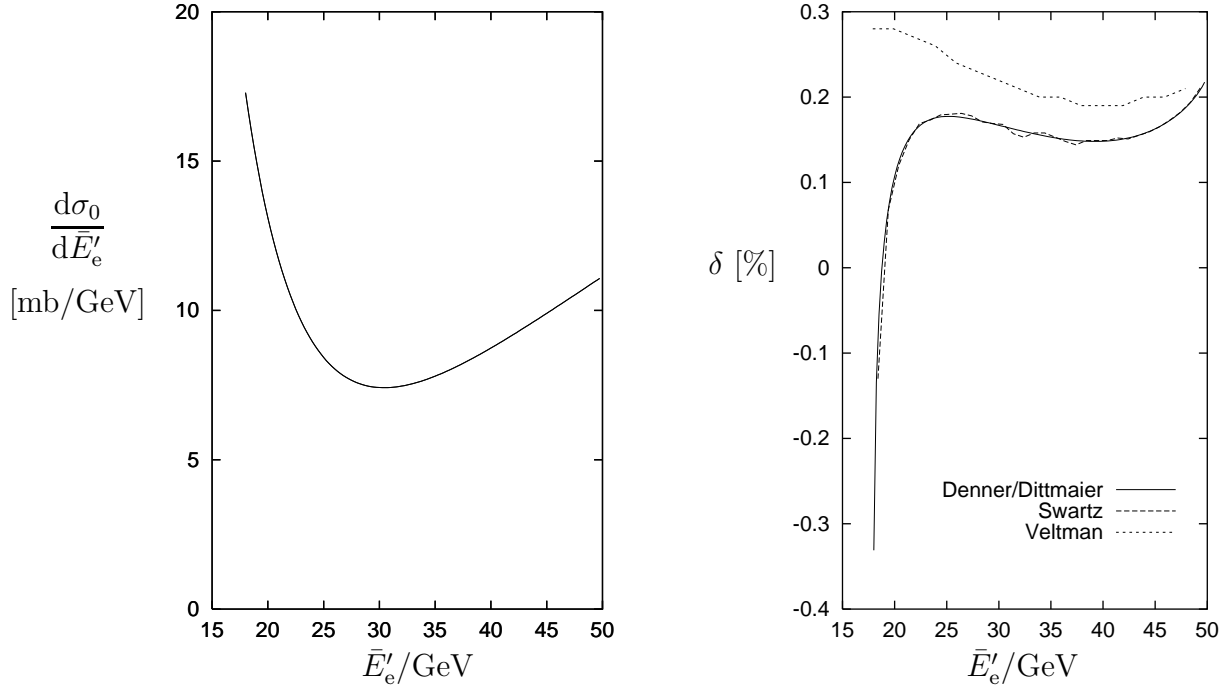


Figure 7: Lowest-order unpolarized cross section (left) and corresponding percentage relative corrections (right) for the SLD polarimeter ($\bar{E}_e = 50$ GeV, $\bar{E}_\gamma = 2.34$ eV)

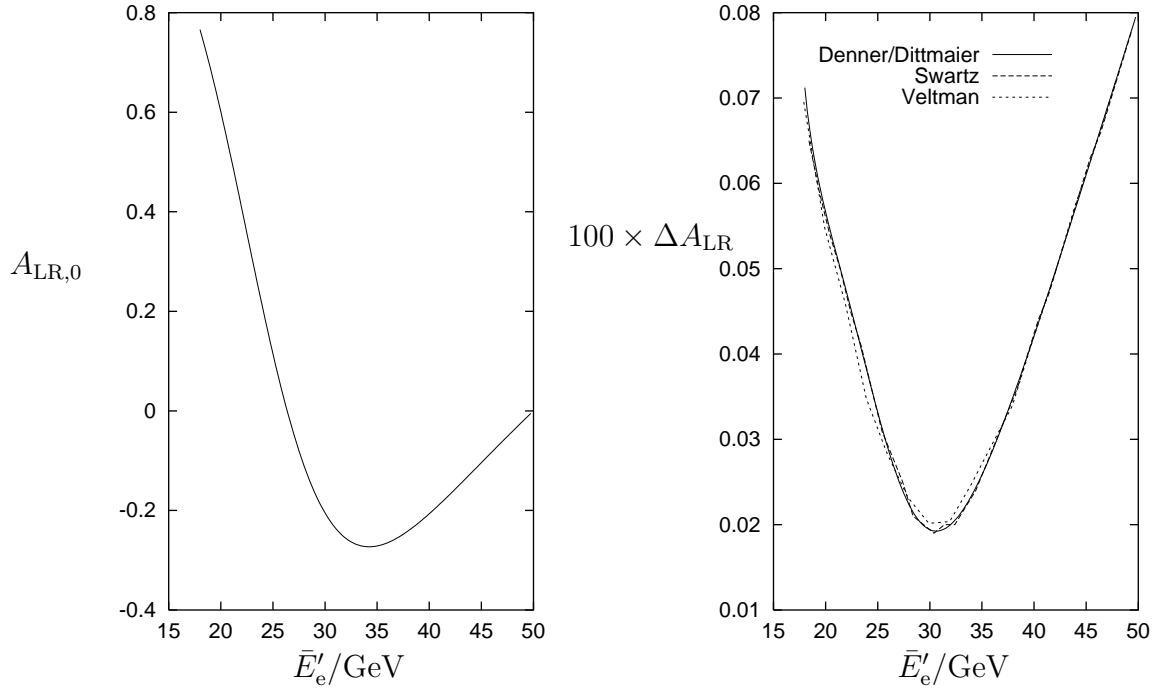


Figure 8: Lowest-order left-right asymmetry (left) and corresponding absolute corrections (right) for the SLD polarimeter ($\bar{E}_e = 50$ GeV, $\bar{E}_\gamma = 2.34$ eV)

\bar{E}'_e [GeV]	$\frac{d\sigma_0}{d\bar{E}'_e} \left[\frac{\text{mb}}{\text{GeV}} \right]$	δ_1 [%]	δ_e [%]	δ_{1e} [%]
50.00	0.50884	0.64	0.42	1.06
100.00	0.25187	0.69	0.74	1.42
150.00	0.17774	0.58	0.66	1.24
200.00	0.14494	0.45	0.71	1.16
250.00	0.12796	0.33	0.95	1.27
300.00	0.11870	0.23	1.33	1.56
350.00	0.11378	0.18	1.41	1.59
400.00	0.11154	0.21	0.00	0.21
450.00	0.11107	0.43	0.00	0.43

Table 5: Lowest-order unpolarized cross section and relative percentage corrections for an NLC polarimeter ($\bar{E}_e = 500$ GeV, $\bar{E}_\gamma = 2.33$ eV)

\bar{E}'_e [GeV]	$A_{\text{LR},0}$	$\Delta A_{\text{LR},1} \times 100$	$\Delta A_{\text{LR},1e} \times 100$	$\delta_{A,1}$ [%]	$\delta_{A,1e}$ [%]
50.00	0.0094	-0.065	-0.201	-6.92	-21.4
100.00	-0.5879	-0.003	0.288	0.01	-0.49
150.00	-0.7047	0.113	0.417	-0.16	-0.59
200.00	-0.6740	0.195	0.470	-0.29	-0.70
250.00	-0.5820	0.240	0.522	-0.41	-0.90
300.00	-0.4649	0.261	0.530	-0.56	-1.14
350.00	-0.3409	0.271	0.397	-0.80	-1.16
400.00	-0.2193	0.284	0.284	-1.29	-1.29
450.00	-0.1050	0.309	0.309	-2.95	-2.95

Table 6: Lowest-order asymmetry and corresponding absolute corrections for an NLC polarimeter ($\bar{E}_e = 500$ GeV, $\bar{E}_\gamma = 2.33$ eV)

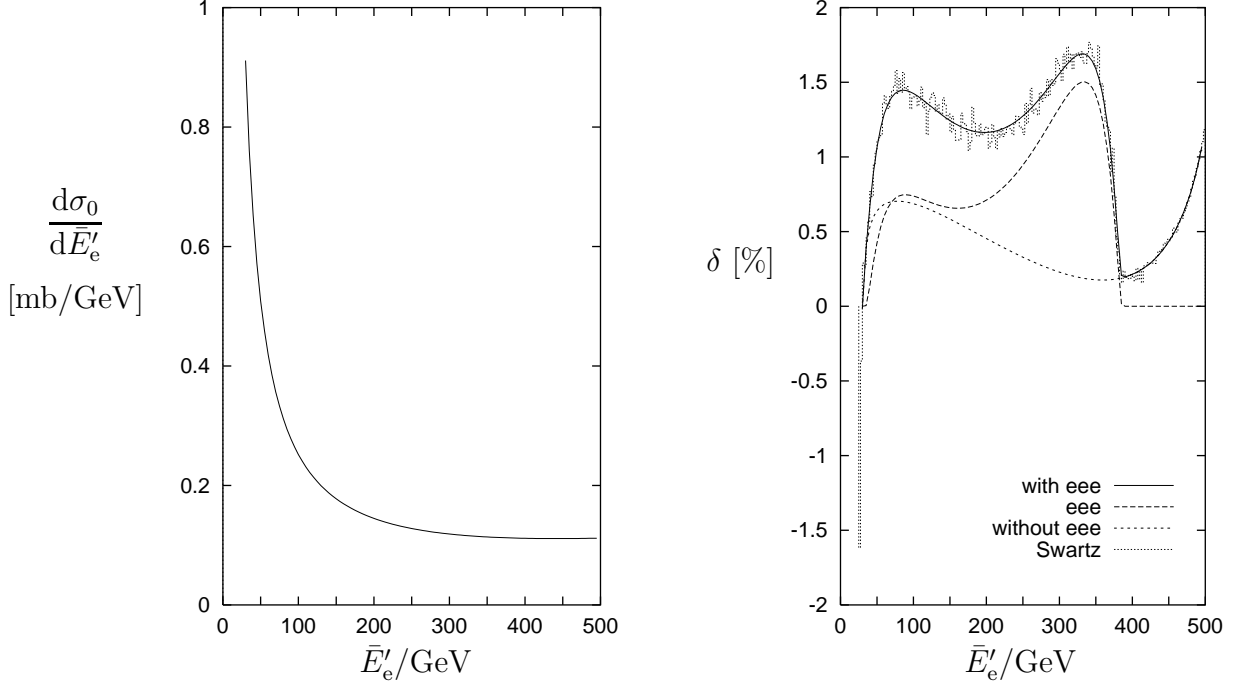


Figure 9: Lowest-order unpolarized cross section (left) and corresponding percentage relative corrections (right) for an NLC polarimeter ($\bar{E}_e = 500$ GeV, $\bar{E}_\gamma = 2.33$ eV)

Moreover, we include the sum of both relative corrections, $\delta_{1e} = \delta_1 + \delta_e$. In addition, we give the corrections to the asymmetry with, $\Delta A_{LR,1e}$, and without, $\Delta A_{LR,1}$, the contributions of the process $e^- \gamma \rightarrow e^- e^- e^+$. The corrections to the unpolarized cross section reach up to 1.7% and contain an essential contribution from $e^- \gamma \rightarrow e^- e^- e^+$. The absolute corrections to the asymmetry are about 5×10^{-3} ; at least half of the effect comes from $e^- \gamma \rightarrow e^- e^- e^+$. Since the relative corrections to the asymmetry amount to 1% of the lowest-order asymmetry, they must be included in precision determinations of the beam polarization at the NLC. For the total unpolarized cross sections we obtain

$$\sigma_0 = 88.103 \text{ mb}, \quad \delta_1 = 0.44\%, \quad \delta_e = 0.29\%, \quad \delta_{1e} = 0.72\%, \quad (5.14)$$

and the results for the related asymmetry are

$$\begin{aligned} A_{LR,0} = -0.2593, \quad \Delta A_{LR,1} = 0.00044, \quad \Delta A_{LR,1e} = 0.00047, \\ \delta_{A,1} = -0.17\%, \quad \delta_{A,1e} = -0.18\%. \end{aligned} \quad (5.15)$$

Swartz [12] has considered the same kind of NLC polarimeter. In Figs. 9 and 10 we compare our results with his findings. We can fully confirm his results, the variation of which is a measure of the Monte Carlo integration error. Note that we use a direct Monte Carlo integration of the differential cross section, while he is using an event generator.

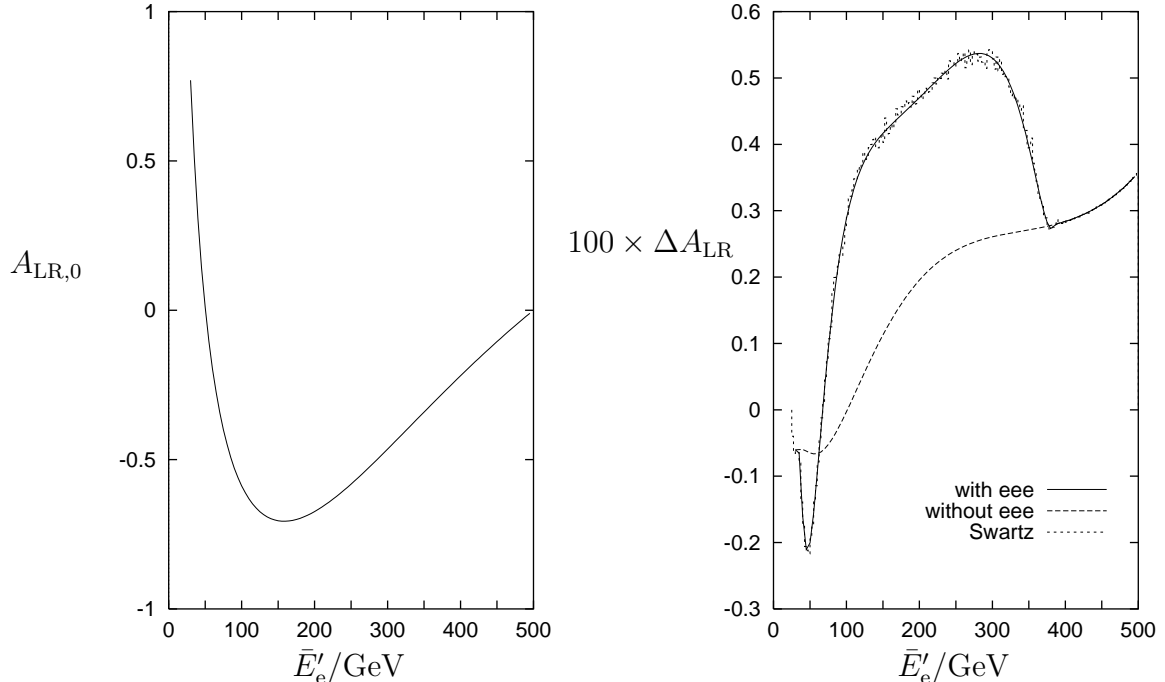


Figure 10: Lowest-order left–right asymmetry (left) and corresponding absolute corrections (right) for an NLC polarimeter ($\bar{E}_e = 500$ GeV, $\bar{E}_\gamma = 2.33$ eV)

6 Conclusion

In present and future e^+e^- colliders the polarization of the initial-state particles plays a fundamental role. One way to measure this polarization is by using Compton backscattering. Because of the use of lasers, the relevant centre-of-mass (CM) energies are in the MeV region, i.e. of the order of the electron mass. The use of such a Compton polarimeter requires the knowledge of the Compton process with sufficient accuracy, i.e. radiative corrections must be controlled.

The genuinely weak corrections are negligible, because the relevant energies are small with respect to the electroweak scale. We have calculated the complete virtual, soft-photon, and hard-photon radiative QED corrections to the process $e^-\gamma \rightarrow e^-\gamma$ for arbitrarily polarized photons and electrons, including the electron mass throughout. A very simple approximation for the corrections to the polarization asymmetry for small CM energies has been presented. We have also calculated the cross section for $e^-\gamma \rightarrow e^-e^-e^+$, which contributes to the corrections for high-energy electron beams. For the processes $e^-\gamma \rightarrow e^-\gamma\gamma$ and $e^-\gamma \rightarrow e^-e^-e^+$ we have constructed analytical results for the matrix elements and determined the integrated cross section by Monte Carlo integration. We have presented all results in a form as simple as possible and written all necessary formulas in a transparent way. This facilitates the use of our results and computer programs by our experimental colleagues.

We have applied our programs to three different situations: the CEBAF polarimeter, which detects the energy of the scattered photon(s), the SLD polarimeter, which detects the energy of the scattered electron, and a polarimeter for a Next Linear Collider (NLC)

that is similar to the one for the SLD, which cannot distinguish between electrons from the processes $e^- \gamma \rightarrow e^- \gamma \gamma$ and $e^- \gamma \rightarrow e^- e^- e^+$. While the relative corrections to unpolarized cross sections are suppressed for low CM energies, there is no such suppression for the relative corrections to the polarization asymmetry. For CM energies that are relevant to the CEBAF and SLD polarimeters we find corrections to the asymmetry of the order of a few 0.1%, whenever it is sizeable. For an NLC polarimeter with an electron beam energy of 500 GeV we find corrections at the 1% level; in this case the process $e^- \gamma \rightarrow e^- e^- e^+$ contributes significantly.

We have compared our results for the SLD polarimeter with those of H. Veltman and Swartz, which are not in mutual agreement. Between their results there are significant deviations for the unpolarized cross section and small discrepancies for the polarization asymmetry. We find complete agreement with the results of the generator COMRAD by Swartz for the NLC and SLD polarimeters. Thus, our code provides, besides the generator COMRAD, a second completely independent program for the electromagnetic corrections to polarized Compton scattering. Our code can be adapted also to other situations, e.g. to transversely polarized e^\pm beams.

Appendix

Effects from a non-zero incident-beam angle

In this paper we have consistently neglected the small angle α_c between the electron and photon beam axes. To justify this procedure, we have calculated the lowest-order cross sections and the polarization asymmetry also for α_c different from zero. For angles α_c typically of order 10^{-2} rad, we find corrections to the results for $\alpha_c = 0$ that are at least one order of magnitude smaller than the ones induced by the radiative corrections discussed in this paper. In the following we briefly sketch the modifications that are necessary to generalize the lowest-order formulas to non-zero α_c .

There are two different origins of modifications induced by $\alpha_c \neq 0$. First, of course the kinematics is changed. Secondly, owing to the acollinearity of the beam axes in the LAB frame, the Lorentz transformation to the CM system is no longer a simple boost along the electron direction of flight and thus involves also a spin rotation of the incoming electron.

We start by considering the kinematics. Identifying the z axis in the LAB frame with the electron beam axis, the incoming momenta are

$$p^\mu = \bar{E}_e(1, 0, 0, \bar{\beta}), \quad k^\mu = \bar{E}_\gamma(1, 0, -\sin \alpha_c, -\cos \alpha_c), \quad (\text{A.1})$$

leading to

$$s = m_e^2 + 2\bar{E}_\gamma \bar{E}_e(1 + \bar{\beta} \cos \alpha_c). \quad (\text{A.2})$$

We decompose the Lorentz transformation from the LAB frame to the CM system into three steps: step (i) is a rotation about the x axis with angle $-\omega_1$, which orients the spatial part of the total incoming momentum $p + k$ along the positive z axis. Step (ii) is a boost along the (new) negative z direction; its strength β_b is chosen to lead us to the CM system. Step (iii) is a rotation about the resulting x axis with angle ω_2 , orienting the

spatial parts of the incoming particle momenta along the z axis in the CM system. The components of p and k in the CM system are the same as in (2.3). These considerations fix the parameters β_b and ω_i to

$$\gamma_b = \frac{1}{\sqrt{1 - \beta_b^2}} = \frac{\bar{E}_e + \bar{E}_\gamma}{\sqrt{s}}, \quad \sin \omega_1 = \frac{\bar{E}_\gamma \sin \alpha_c}{\beta_b(\bar{E}_e + \bar{E}_\gamma)}, \quad \sin \omega_2 = \frac{\bar{\beta} \sin \alpha_c}{\gamma_b \beta_b (1 + \bar{\beta} \cos \alpha_c)}. \quad (\text{A.3})$$

From this representation we can already read that $\omega_{1,2}$ are both of $\mathcal{O}(\alpha_c)$ and that they are additionally strongly suppressed by the small factors \bar{E}_γ/\bar{E}_e and γ_b^{-1} , respectively.

Since the rotational invariance about the electron beam axis is lost, we have to include azimuthal angles $\bar{\phi}'_e$ and ϕ'_e in the momentum p' of the outgoing electron, as specified in (4.3). The relation between the electron energy \bar{E}'_e in the LAB frame and the electron angles θ'_e , ϕ'_e in the CM system is given by

$$\bar{E}'_e = E_e \gamma_b [1 + \beta_b \beta (\cos \omega_2 \cos \theta'_e - \sin \omega_2 \sin \theta'_e \sin \phi'_e)]. \quad (\text{A.4})$$

The CM quantities E_γ , E_e , and β are related to s as in (2.2) and (2.4). In order to calculate unpolarized cross sections in the LAB frame, the spin-averaged squared amplitude, $\langle |\mathcal{M}|^2 \rangle$, has to be known. Note that $\langle |\mathcal{M}|^2 \rangle$ is a Lorentz-invariant function of the Mandelstam variables s , t , u , and thus that it does not depend on ϕ'_e when expressed in terms of CM quantities. Therefore, the unpolarized cross section σ_0 does not explicitly depend on ϕ'_e either. For the distribution $d\sigma_0/d\bar{E}'_e$ we obtain

$$\frac{d\sigma_0}{d\bar{E}'_e} = \frac{1}{E_\gamma \gamma_b \beta_b} \int_0^{2\pi} d\psi \frac{d^2\sigma_0}{d\phi'_e d\cos \theta'_e}, \quad \bar{E}'_e \geq E_e \gamma_b (1 \mp \beta_b \beta), \quad (\text{A.5})$$

where the auxiliary variable ψ determines the scattering angle θ'_e ,

$$\cos \theta'_e = \left(\frac{\bar{E}'_e - E_e \gamma_b}{E_\gamma \gamma_b \beta_b} \right) \cos \omega_2 + \sqrt{1 - \left(\frac{\bar{E}'_e - E_e \gamma_b}{E_\gamma \gamma_b \beta_b} \right)^2} \cos \psi \sin \omega_2, \quad (\text{A.6})$$

which plays the role of the scattering angle θ in (2.4). The integration over ψ is related to the integration over the azimuthal angle ϕ'_e in the CM system via

$$\sin \phi'_e = \frac{1}{\sin \theta'_e} \left[\sqrt{1 - \left(\frac{\bar{E}'_e - E_e \gamma_b}{E_\gamma \gamma_b \beta_b} \right)^2} \cos \psi \cos \omega_2 - \left(\frac{\bar{E}'_e - E_e \gamma_b}{E_\gamma \gamma_b \beta_b} \right) \sin \omega_2 \right]. \quad (\text{A.7})$$

Owing to (A.4) this integration includes an averaging process over θ'_e when \bar{E}'_e is kept fixed for $\alpha_c \neq 0$. For $\alpha_c = \omega_i = 0$ the angle θ'_e is fully determined by \bar{E}'_e [see (2.13)], and the integration over ψ yields a factor 2π .

These considerations show that a finite α_c affects the unpolarized cross section through the CM energy \sqrt{s} , which is changed in $\mathcal{O}(\alpha_c^2)$ and enters all kinematical variables, and via the auxiliary angles ω_i , where the effects are of $\mathcal{O}(\alpha_c)$ but additionally suppressed by at least a factor of γ_b^{-1} .

For the calculation of polarized cross sections one has to take into account the spin rotations of the electrons. In the following we only consider the polarization of the incoming

electron and assume spin summation for the final-state electron. Denoting Dirac spinors and amplitudes with spin $\sigma = \pm\frac{1}{2}$ in the CM system by $u(\alpha_c, \sigma)$ and $\mathcal{M}(\alpha_c, \sigma)$, respectively, the relations between the amplitudes with $\alpha_c = 0$ and $\alpha_c \neq 0$ read

$$\mathcal{M}(\alpha_c, \sigma) = \sum_{\tau=\pm} \mathcal{M}(\alpha_c = 0, \tau) A_{\tau\sigma}, \quad A_{\tau\sigma} = \frac{1}{2m_e} \bar{u}(\alpha_c = 0, \tau) u(\alpha_c, \sigma). \quad (\text{A.8})$$

The components of the unitary matrix A are given by

$$A_{\pm\mp} = \frac{-im_e \sin \frac{\alpha_c}{2}}{\bar{E}_e \sqrt{(1+\bar{\beta})(1+\bar{\beta} \cos \alpha_c)}}, \quad A_{\pm\pm} = \sqrt{1 - |A_{+-}|^2}. \quad (\text{A.9})$$

The deviation of A from the identity matrix is very small. The off-diagonal elements are of $\mathcal{O}(\alpha_c)$ times the suppression factor of m_e/\bar{E}_e , which is even smaller than γ_b^{-1} . The deviation of the diagonal elements from 1 is of the order of the square of the off-diagonal elements.

In conclusion, we find that the influence of an angle $\alpha_c \neq 0$ on the Compton cross sections and the polarization asymmetry is at most of the relative order of α_c^2 or $\alpha_c \gamma_b$. The above analytical considerations have also been checked numerically.

Acknowledgements

We thank C. Grosse-Knetter for participating in the early stage of this work. Moreover, we are grateful to C. Cavata and M.L. Swartz for helpful information about the CEBAF and SLD polarimeters, respectively. We thank M.L. Swartz also for providing us with explicit numbers of the results presented in Ref. [12].

References

- [1] SLD Collaboration, K. Abe et al., *Phys. Rev. Lett.* **70** (1993) 2515, **73** (1994) 25, and **78** (1997) 2075;
R.E. Frey, OREXP 97-03, hep-ex/9710016.
- [2] G. Bardin et al., *Conceptual Design Report of a Compton Polarimeter for CEBAF Hall A*, SACLAY internal report DAPNIA-SPhN-96-14.
- [3] J.P. Jorda, *A 4–8 GeV Compton Polarimeter for TJNAF*, SACLAY internal report DAPNIA-SPhN-96-42.
- [4] G. Bardin, C. Cavata and J.P. Jorda, *Compton Polarimeter Studies for TESLA*, DESY-TESLA-97-03.
- [5] W. Thirring, *Phil. Mag.* **41** (1950) 1193;
J.D. Bjorken and S.D. Drell, *Relativistic Quantum Fields* (McGraw-Hill, New York, 1965).
- [6] S. Dittmaier, *Phys. Lett.* **B409** (1997) 509.

- [7] L.M. Brown and R.P. Feynman, *Phys. Rev.* **85** (1952) 231.
- [8] F. Mandl and T.H.R. Skyrme, *Proc. Roy. Soc.* **A215** (1952) 497.
- [9] K.A. Milton, W. Tsai and L.L. De Raad, *Phys. Rev.* **D6** (1972) 1411 and **D6** (1972) 1428.
- [10] A. Góngora-T. and R.G. Stuart, *Z. Phys.* **C42** (1989) 617.
- [11] H. Veltman, *Phys. Rev.* **D40** (1989) 2810; E: *ibid.* **D42** (1990) 1856.
- [12] M.L. Swartz, SLAC-PUB-7701, hep-ph/9711447.
- [13] A. Denner and S. Dittmaier, *Nucl. Phys.* **B407** (1993) 43.
- [14] S. Dittmaier, *Nucl. Phys.* **B423** (1994) 384.
- [15] S. Dittmaier, CERN-TH/98-143, hep-ph/9805445.
- [16] A. Denner, *Fortschr. Phys.* **41** (1993) 307.
- [17] G. Passarino and M. Veltman, *Nucl. Phys.* **B160** (1979) 151.
- [18] G. 't Hooft and M. Veltman, *Nucl. Phys.* **B153** (1979) 365;
W. Beenakker and A. Denner, *Nucl. Phys.* **B338** (1990) 349.
- [19] J. Küblbeck, M. Böhm and A. Denner, *Comput. Phys. Commun.* **60** (1990) 165;
H. Eck and J. Küblbeck, *Guide to FeynArts 1.0*, University of Würzburg, 1992.
- [20] R. Mertig, M. Böhm and A. Denner, *Comput. Phys. Commun.* **64** (1991) 345;
R. Mertig, *Guide to FeynCalc 1.0*, University of Würzburg, 1992.
- [21] A. Denner, S. Dittmaier and M. Stöbel, *Phys. Rev.* **D53** (1996) 44.
- [22] G.P. Lepage, *J. Comp. Phys.* **27** (1978) 192; Cornell University preprint, CLNS-80/447.
- [23] F.A. Berends, P.H. Daverveldt and R. Kleiss, *Nucl. Phys.* **B253** (1985) 441;
R. Kleiss and W.J. Stirling, *Nucl. Phys.* **B262** (1985) 235 and *Phys. Lett.* **179B** (1986) 159;
R. Kleiss, *Z. Phys.* **C33** (1987) 433.
- [24] The LEP collaborations ALEPH, DELPHI, L3, OPAL, the LEP Electroweak Working Group and the SLD Heavy Flavor Group (D. Abbaneo et al.), CERN-PPE/97-154.